Damping Acoustic Pressure Pulsations in Pipelines Using Helmholtz Resonators

by

Karim Sachedina

A Thesis Submitted in Partial Fulfillment
of the Requirements for the Degree of

Master of Applied Science

in
The Faculty of Engineering and Applied Science
Mechanical Engineering

University of Ontario Institute of Technology
Oshawa, Ontario, Canada

May, 2019

Thesis Examination Information

Submitted by Karim Sachedina

Master of Applied Science in Mechanical Engineering

Thesis title: Damping Acoustic Pressure Pulsations in Pipelines Using Helmholtz Resonators

An oral defense of this thesis took place on May 15, 2019 in front of the following examining committee:

Examining Committee:

Chair of Examining Committee	Dr. Sayyed Ali Hosseini
Research Supervisor	Dr. Atef Mohany
Examining Committee Member	Dr. Martin Agelin-Chaab
University Examiner	Dr. Haoxiang Lang

The above committee determined that the thesis is acceptable in form and content and that a satisfactory knowledge of the field covered by the thesis was demonstrated by the candidate during the oral examination. A signed copy of the Certificate of Approval is available from the School of Graduate and Postdoctoral Studies.

Abstract

In industrial piping systems, centrifugal and reciprocating turbomachinery generate acoustic pressure pulsations, which propagate into the pipeline and interact with piping components, potentially causing vibrations, increased fretting wear, and even fatigue failure. In this thesis, an acoustic damping device known as the Helmholtz resonator (HR) is experimentally studied. The effects of HR cavity volume, pipeline diameter, HR location, the use of multiple HRs, and mean flow velocity are investigated to determine their effects on the acoustic attenuation achieved within a pipeline. Measurements are also performed to clarify the mechanism of attenuation and the effects of incident pressure amplitude on the transmission loss of an HR. The findings of this thesis may be used as practical guidelines for the use of HRs in industrial systems, where characterizing the acoustics is usually difficult and costly, and the available space for damping devices may be limited.

Statement of Contributions

The experimental work described in this thesis was performed at the Aeroacoustics and Noise Control Laboratory at the University of Ontario Institute of Technology, under the supervision of Dr. Atef Mohany. I performed the experimental work, analysis, and writing of this thesis. Preliminary findings for the results discussed in Chapter 6 were obtained with the help of Thomas Lato, to whom I am thankful. I have used standard referencing practices to acknowledge ideas, research techniques, and other materials that belong to others. Parts of this thesis work, as described in Chapters 4, 5, and 6, have been submitted for publishing.

Dedication

I dedicate this thesis to everyone who commits themselves to making this world a better place. I hope that you always work towards improving yourself, helping those around you, and following your dreams. I encourage you to pursue your vocations with vigor and moral courage.

"By my love and hope I entreat you: do not reject the hero in your soul! Keep holy your highest hope!"

Friedrich Nietzsche

Philosopher

1844-1900

Acknowledgments

I wish to express my utmost gratitude for the guidance, support, and wisdom of my supervising professor, Dr. Atef Mohany. I am also grateful to my colleagues at the Aeroacoustics and Noise Control Laboratory, including Nadim, Thomas, Moamen, Mohammed, Mahmoud, Rashid, and Omar. Their knowledge, experience, and positive attitudes have been immensely helpful throughout my studies. I would also like to thank Joel, Marsha, and Rachel, the understated heroes of the program who are always supportive of graduate students.

I also thank the CANDU Owners Group (COG), University Network for Excellence in Nuclear Engineering (UNENE), and Natural Science and Engineering Research Council of Canada (NSERC) for the funding that made this work possible.

Finally, I thank my mom, dad, stepdad, brother, and girlfriend for their thoughtfulness and patience. They have encouraged me to pursue studies in a field I am passionate about, to a level I am fortunate to have the opportunity to access. They have imparted a strength that is manifest in the tenacity with which I have laboured for this and any other of my other works. Their love is the source of my inspiration.

Contents

Nomenclature

A	Acoustic pressure antinode
A_n	Cross-sectional area of HR neck (m^2)
A_p	Cross-sectional area of pipe (m^2)
A_v	Cross-sectional area of HR cavity (m^2)
B	Midpoint between A and M
C	Midpoint between M and N
c	Speed of sound (m/s)
c_n	Acoustic damping within HR neck
d	Distance (m)
d_p	Pipe diameter (m)
EC	Expansion chamber
f	Frequency (Hz)
f_a	Acoustic natural frequency (Hz)
f_b	Blade passage frequency (Hz)
f_{HR}	HR natural frequency (Hz)
f_u	Upper frequency limit (Hz)
h	Ratio of cross-sectional areas between pipe and expansion chamber
H	Acoustic transfer function
HR	Helmholtz resonator
IL	Insertion loss (dB)
k	Acoustic wavenumber ($1/m$)
k_c	Stiffness of HR cavity volume (N/m)
L	Length (m)
l_{EC}	Length of expansion chamber (m)
l_{eff}	Effective HR neck length (m)
l_n	HR neck length (m)

l_v	HR cavity length (m)
M	Midpoint between acoustic pressure node and antinode
m	HR neck mass (kg)
N	Acoustic pressure node
n_b	Number of impeller blades
p	Acoustic pressure (Pa)
P_s	Input power to acoustic source (W)
QWR	Quarter wave resonator
R	Acoustic reflection coefficient
r_n	HR neck radius
s	Microphone spacing (m)
SPL	Sound pressure level (dB)
$T_{11}, T_{12}, T_{21}, T_{22}$	Acoustic transfer matrix coefficients
TL	Transmission loss (dB)
v	Acoustic particle velocity (m/s)
V_c	HR cavity volume (m^3)
W	Acoustic power (W)

Greek letters

α	HR neck end correction value (m)
Δ	Matrix determinant
λ	Acoustic wavelength (m)
ϕ	Phase angle (degrees)
ρ	Fluid density (kg/m^3)
ω	Angular frequency ($1/s$)
ω_{shaft}	Rotational speed of shaft (rpm)

List of Tables

List of Figures

Chapter 1

Introduction

1.1 Background and Motivation

Acoustic pressure pulsations in industrial pipeline systems can result in the increased fretting wear or fatigue failure of piping system components. The operation of turbomachinery and the unstable flow at geometric discontinuities within a pipeline generate acoustic waves, which may be amplified depending on the system's damping and geometry. This may result in acoustic resonance, which manifests as a standing wave within the pipeline with pressure magnitudes much higher than the dynamic head of the flow. Many studies have been done regarding the characterization of the acoustic sources in pipeline systems, including centrifugal pumps, compressors, valves, sidebranches, and bluff bodies. This research has largely focused on investigating the parameters that contribute to noise generation and amplification. Other research has been conducted regarding measures to reduce or eliminate the noise that is generated in the pipeline. For example, the effect of pump parameters such as the volute tongue shape and blade profile have been considered to determine the optimal geometries to reduce pressure pulsation amplitudes. For flow-excited oscillations, measures for disrupting the feedback mechanism between the unstable flow and the sound field have been considered, such as the use of spoilers at

the edge of sidebranches or cavities and the use of mass injection at the point of shear layer separation.

However, it may be unrealistic to eliminate the source of acoustic excitation. This is the case with centrifugal and reciprocating turbomachinery, which are necessary for flow and pressure requirements in piping systems, but necessarily create discrete acoustic pulses by virtue of their mechanism of operation. It is therefore of interest to investigate methods that can significantly reduce the transmission of acoustic waves from the source and that can be incorporated into existing systems with minimal interference logistically and operationally. This thesis investigates the use of a passive damping device known as the Helmholtz resonator (HR) for acoustic attenuation in piping systems. While HRs have been studied in some depth in the literature, their incorporation into industrial pipelines is often difficult because of the host of complicating factors that exist in industry, such as the need to achieve high levels of acoustic damping, spatial limitations, and the presence of mean flow. Therefore, the main objective of this thesis is to determine the effects of various parameters that affect the applicability of Helmholtz resonators to industrial systems, as discussed below.

1.2 Scope of Work

To fulfill the objective of this thesis, an experimental pipeline setup was constructed to allow for the evaluation of damping devices in different configurations. A modular test section was used, which allowed both acoustically resonant, i.e. standing wave, and off-resonant, i.e. travelling wave, scenarios to be studied. Circular concentric Helmholtz resonators of various dimensions were tuned to target 150 Hz, which was selected as the frequency of interest. Transmission loss and insertion loss measurements were taken to evaluate the acoustic damping of HRs in various arrangements and flow conditions. First, the effects of HR and pipeline volume were investigated to determine the scalability of

HRs to various systems. Second, the effects of axial location were considered, to determine the sensitivity of HR acoustic performance on placement within a pipeline system. Third, the use of multiple HRs was studied to determine the HR arrangements that yield maximal damping. Lastly, the effects of both mean flow velocity and directionality were studied to determine the feasibility of incorporating HRs into systems with mean flows.

To understand some of the trends seen for the acoustic damping, the mechanism of attenuation of HRs was studied using pressure, phase, and reflection coefficient measurements. First, the mechanism of attenuation of a single sidebranch HR was investigated using transfer function measurements between the HR cavity and the main pipeline at the HR junction. For multiple HRs with various axial spacing distances, reflection coefficient measurements were taken to determine the amount of reflected acoustic energy. Transfer function measurements between the HR cavities of two HRs with different spacing distances were then taken to determine the relative amplification within each HR, i.e. the relative amount of energy absorbed from the pipeline.

Finally, the effect of acoustic pressure amplitude on the response of the Helmholz resonator is discussed. Transmission loss measurements of multiple devices, including an HR, expansion chamber, and quarter wave resonator, are made for various excitation levels. The results are compared to determine the sensitivity of the various damping devices to the amplitudes of acoustic excitation.

1.3 Thesis Outline

Following this introduction, which provides a brief discussion of the background, objectives, and scope of work, Chapter 2 presents a discussion of the relevant literature regarding acoustic excitation in pipelines and noise control methods. Chapter 3 provides an overview of the experimental setup used and the methodologies employed for analysis. In Chapter 4, the results regarding the acoustic damping of various HRs in multiple con-

figurations are discussed. The effects of HR and pipeline volume, axial location, multiple HRs, and mean flow velocity and directionality are discussed from the perspective of acoustic attenuation. Chapter 5 presents experimental results for pressure, phase, and reflection coefficient measurements, which were performed in order to clarify the mechanism of attenuation of the Helmholtz resonator. In Chapter 6, the effects of acoustic pressure amplitude on the acoustic damping achieved by HRs is discussed. Chapter 7 provides a brief summary of the findings and presents the overall conclusions.

Chapter 2

Literature Review

2.1 Acoustic Excitation in Piping Systems

Acoustic waves are oscillations in pressure, i.e. compressions and rarefactions, that oscillate in the same direction as they travel. These longitudinal waves propagate at the speed of sound, which is determined by the properties of the medium they are passing through, namely the bulk modulus and density [1]. Generally, acoustic waves can be characterized using the sound pressure and particle velocity. The frequency and wavelength of acoustic waves can be related to the speed of sound using $f = c/\lambda$, where f is frequency, c is the speed of sound, and λ is the wavelength. Acoustic waves can propagate, reflect, and interfere with one another in pipeline systems. The characteristics of the acoustics in a pipeline system depend upon the frequencies and magnitudes of excitation, the fluid(s) used in the piping, the levels of damping in the system, and the pipeline material, geometry, and boundary conditions .

If the wavelengths of acoustic excitation are greater than the diameter of the pipeline, it can be assumed that the acoustic waves are one-dimensional, i.e. that they propagate along the axial direction of the pipe. In this case, the acoustic pressure will be the same at any point within a cross-section of the pipe. This is true for several cases in

industry, where the relatively low frequencies from turbomachinery result in acoustic waves with wavelengths much larger than the pipe diameter. The upper frequency limit for assuming plane, or one-dimensional, wave propagation is defined in ASTM E2611 [2] as $f_u < 0.586c/d_p$, where f_u is the upper frequency limit and d_p is the pipe diameter. Reflections of the acoustic waves will occur at the end terminations of the piping, unless the termination is anechoic, which results in an interaction between incident and reflected waves. The pipeline length, end terminations, system damping, and speed of sound of the working fluid will determine which frequencies are amplified or attenuated as a result of this interaction.

The excitation frequencies that will be maximally amplified within a given pipeline system are known as the acoustic natural frequencies, f_a. If the acoustic excitation matches an acoustic natural frequency of the piping system, and there is sufficient energy to overcome the system damping, acoustic resonance occurs, which manifests as a standing wave. A schematic of the pressure distribution of the first few longitudinal resonant modes in a pipe with both its ends open is shown in Figure 2.1. The wavelengths and frequencies of each mode are shown in terms of the pipe length, L, and the speed of sound, c [1]. It can be seen that the open end acts as an acoustic pressure node, where there is no pressure oscillation. Acoustic pressure antinodes, where the pressure oscillates with high magnitudes, are formed in other locations along the pipeline, according to the corresponding mode. The first three longitudinal modes for a pipe with one end closed and the other open is shown in Figure 2.2. The closed end boundary acts as an acoustic pressure antinode, which results in a shift of the resonant frequencies from the open-open pipe. These schematics illustrate the effect of pipeline length and boundary conditions on the acoustic resonant modes.

If the acoustic excitation does not correspond to an acoustic natural frequency of the piping, or if there is high system damping, the acoustic waves will simply propagate along the length of the pipeline. In this case, there is no coupling between the pipeline

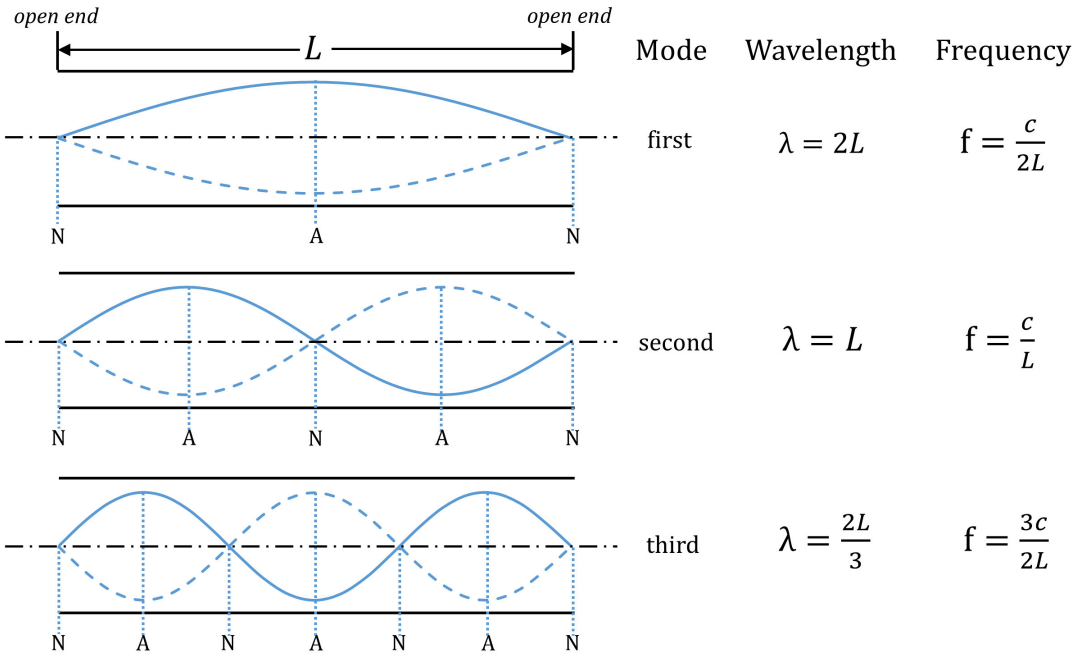

Figure 2.1: Schematic of acoustic pressure distribution of first three longitudinal modes of an open-open pipeline.

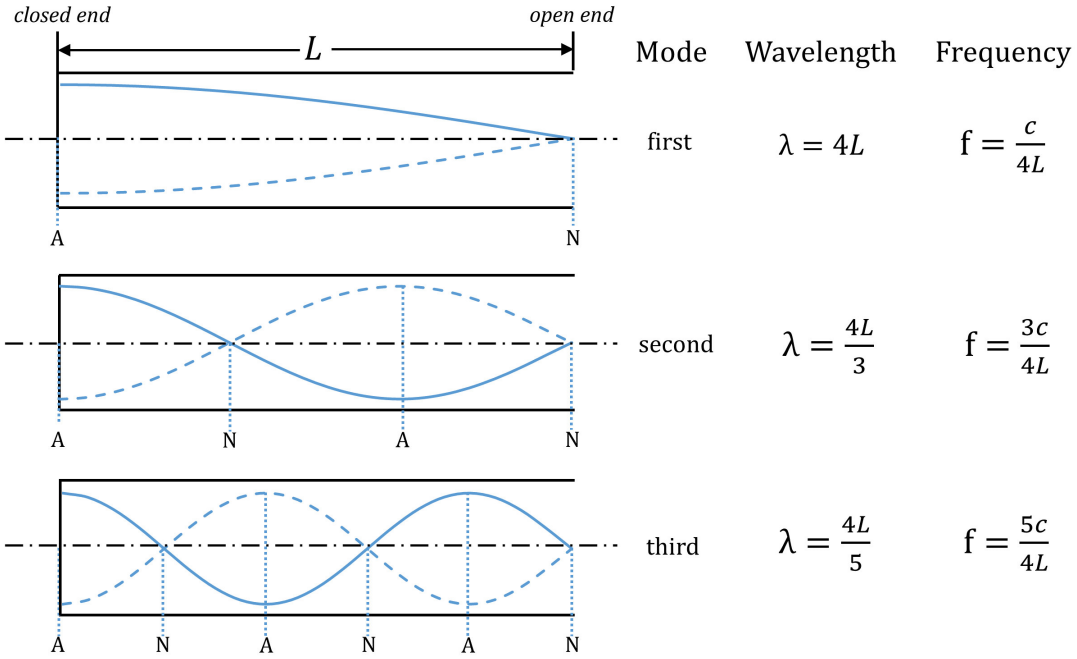

Figure 2.2: Schematic of acoustic pressure distribution first three longitudinal modes of a closed-open pipeline.

and fluid properties and the acoustic excitation. The amplitudes of these acoustic waves will be lower than those of a resonant condition, but will nonetheless interact with piping system components, potentially causing increased fretting wear or fatigue failure [3, 4]. Approximating the amplitudes of acoustic excitation in industrial pipelines is therefore critical for determining whether they are within acceptable levels.

Acoustic damping is significant because the maximum pressure amplitudes achieved in a system are limited by damping. The acoustic damping of plane waves in pipelines has been investigated by, among others, Kirchhoff [5], Peters et al. [6], and Dokumaci [7]. Generally, the damping is caused by viscothermal losses, which refers to losses in the acoustic boundary layer and the interaction between the acoustic field and mean flow. However, while models exist that can accurately predict the damping of acoustic waves as they propagate unidirectionally through a pipe, the acoustic pressures in a pipeline are a result of both forward and backward propagating waves, for which damping also exists in the form of losses at the boundary conditions [8]. Additionally, the multitude of pipeline components, such as connection points and valves, affect the acoustic response of industrial piping systems, further complicating their acoustic analysis. It has also been found that elevated temperatures and pressures affect the acoustic damping in pipes [9]. The magnitudes of acoustic pressure in a pipeline system are therefore difficult to predict, especially for resonant systems. The following sections discuss the sources of acoustic excitation in industrial piping.

2.1.1 Flow instability and feedback mechanisms

Flow instabilities at geometric discontinuities in system piping can result in the generation of noise. The main types of flow-excited mechanisms that generate acoustic excitation can be categorized into fluid-dynamic, fluid-resonant, and fluid-elastic oscillations according to Rockwell and Naudascher [10]. The mechanism of fluid-dynamic oscillations can be understood by referring to Figure 2.3, which shows a schematic of the flow over a cavity.

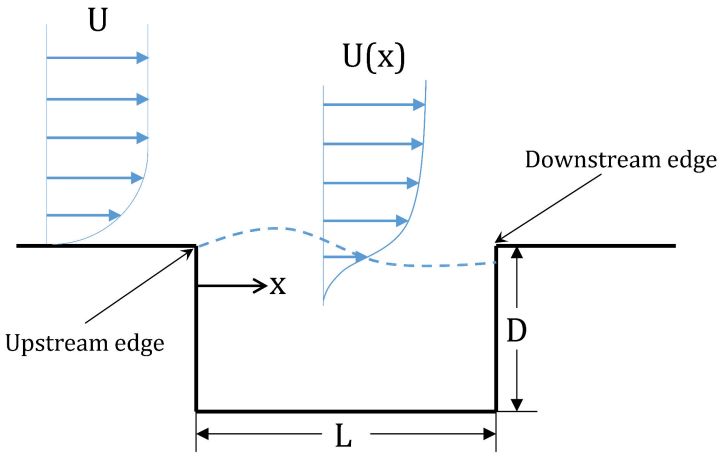

Figure 2.3: Schematic of shear layer separation over the mouth of a cavity with length L and depth D.

As the flow passes over the cavity opening, or mouth, it separates into an unstable shear layer. The interaction of this shear layer with the geometry of the cavity and piping can result in the various feedback mechanisms. Fluid-dynamic oscillations occur when the impingement of the shear layer at the downstream edge results in pressure perturbations, or sound waves, which then propagate upstream and enhance the subsequent shear layer separation at the upstream edge, closing the feedback loop. This is shown schematically in Figure 2.4. The mechanism of fluid-resonant oscillations is shown in Figure 2.5. The shear layer over the cavity opening rolls into discrete vortices, and if the acoustic natural frequency of the enclosure matches the frequency of shear layer oscillation (and there is enough energy to overcome the system damping), a feedback mechanism is initiated. The shear layer oscillations act as an acoustic source, initiating the acoustic resonance, and, in turn, the acoustic resonant field enhances the shear layer oscillations. The third flow-excited mechanism is fluid-elastic, whereby the flow couples with an elastic boundary, such as a flexible lower cavity wall.

Much research has been devoted to understanding the mechanism of flow-excited oscillations and control methods for this type of excitation. This includes studies of flow

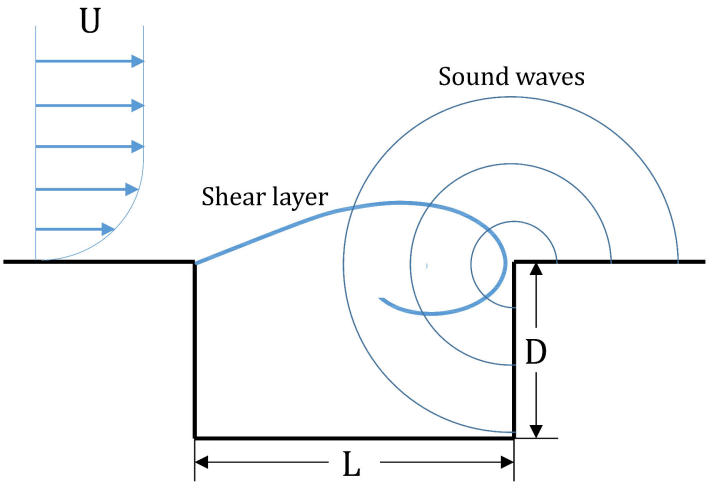

Figure 2.4: Schematic of fluid-dynamic oscillations over a cavity.

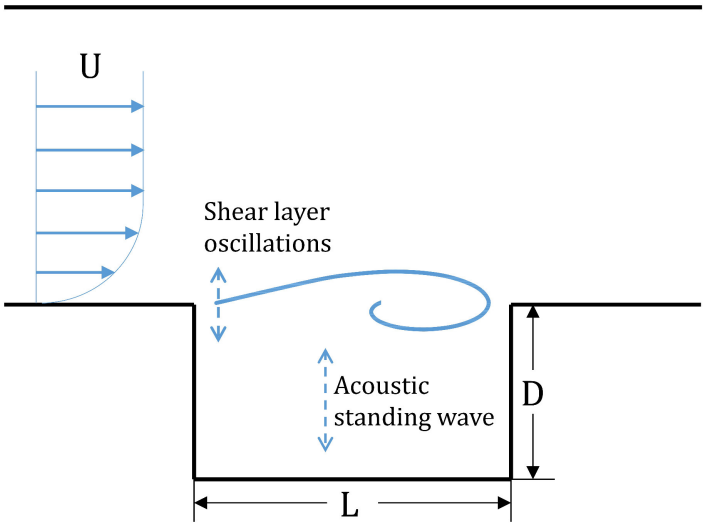

Figure 2.5: Schematic of fluid-resonant oscillations within a confined cavity.

over cavities [10, 11, 12] and side branches [13], jet flows [14], and flow over bluff bodies [15, 16, 17, 18, 19]. Both active and passive methods have been considered for the control of these oscillations. Since flow-excited oscillations are caused by an upstream separation coupled with either flow impingement or a resonance of the system, active control of this upstream separation can be used to control the excitation. For example, the use of synthetic jets at or near the location of flow separation considered by Ziada [20] was

shown to be very effective in disrupting the feedback mechanism. Passive solutions have also been considered, such as those used for the control of flow-excited acoustic resonance of a cavity by Omer et al. [21]. In this case, the downstream edge geometry was modified to affect the impingement point of the shear layer and disrupt the feedback mechanism.

2.1.2 Acoustic pressure pulsations generated by turbomachinery

The second source of acoustic excitation is rotating or reciprocating turbomachinery [22]. For example, acoustic pulses are created in reciprocating pumps due to the intermittent discharge of fluid from the pump [4, 23]. The excitation frequency is therefore associated with the rate at which the valves operate at the discharge side(s) of the cylinder. Acoustic pulsations are also created by centrifugal pumps. As the impeller blades pass over the discharge side of the pump and interact with the volute tongue, pulsations are created which propagate into the adjacent pipeline system [24]. These pulses are generated at the 'blade passing frequency', f_b, which is dependent upon the number of impeller blades and the operation speed of the driven shaft, i.e.

$$f_b = \frac{\omega_{shaft} \cdot n_b}{60} \tag{2.1}$$

where ω_{shaft} is the rotational speed of the pump, in revolutions per minute, and n_b is the number of impeller blades.

The acoustic excitation due to centrifugal turbomachinery is therefore a discrete excitation at the blade passing frequency. However, while the frequency of excitation is readily predicted, it is much more difficult to predict the amplitudes of pressure pulsations created by this mechanism. Acoustic resonance occurs when the blade passage frequency matches an acoustic natural frequency of the attached piping system, i.e. $f_b = f_a$, and there is enough energy to overcome the system damping. One notable example of

this is the failure of fuel bundles at the Darlington Nuclear Generation Station in 1990, which was caused by a coupling between the excitation from the Primary Heat Transport (PHT) pumps and a natural frequency of the piping [24, 25]. This resonance caused acoustic pulses generated by the PHT pumps to be amplified to levels high enough to cause cracks in end plates and elements in the fuel bundles to break loose. In order to eliminate the resonant condition, the number of impeller blades was changed from five to seven, shifting the excitation frequency from 150 Hz to 210 Hz, thereby decoupling the excitation from the natural frequency of the system.

Studies have also revealed that pump properties, such as the cutwater geometry, blade trailing edge profile, operation point, and acoustic impedance of the pump all have an effect on the amplitudes of excitation. Morgenroth and Weaver [24] studied the generation of sound by a centrifugal pump at the blade passing frequency, and found that the peak acoustic pressure at resonance was lowest at the best efficiency point of the pump. It was also observed that rounding the cutwater tip, while maintaining the clearance between the impeller and the cutwater, reduced the amplitudes of the acoustic pressure fluctuations without any noticeable effect on pump performance. Gao et al. [26] found that the geometry of the blade trailing edge profile of the impeller blades contributes to the magnitudes of the generated acoustic pressure pulsations. This was attributed to the reduction in vorticity caused by the interaction between the impellers and volute tongue for certain trailing edge geometries.

Rzentkowski and Zbroja [27] experimentally investigated the acoustics of a double-volute CANDU heat transport pump. The pressure at the discharge side of the pump was measured and the results in the frequency spectra are shown in Figure 2.6. It is clear that the blade passage frequency of 150 Hz has the highest magnitude in the pressure spectrum. The mechanism of acoustic excitation was attributed to the blade-cutwater interaction and the non-uniform outflow from the impeller, but it was noted that the acoustic sources of pumps are highly dependent upon their geometry and operating

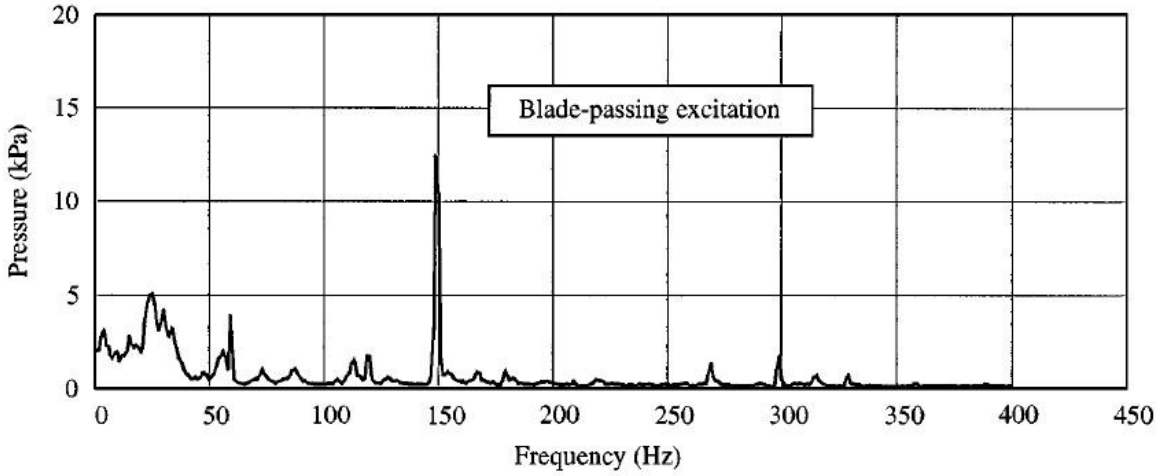

Figure 2.6: Acoustic pressure spectra at discharge side of centrifugal pump, from Rzentkowski and Zbroja [27].

point. For example, it was also found that the temperature highly affects the excitation amplitudes at the blade passing frequency, which is caused by a change in the acoustics of the test loop with a change in temperature.

Research into the characterization of centrifugal pumps has shown the significance of pump parameters and operation points on the magnitudes of acoustic excitation. While this research has shown methods of reducing the acoustic pressure amplitudes, it has also shown that the generation of acoustic pulses is inherent in the operation of centrifugal pumps. It is therefore of interest to investigate methods of reducing the amplitudes of these pressure pulsations in order to mitigate their effect on pipeline system components. The following section highlights some of the methods that have been investigated for damping noise in pipeline or duct systems, with a specific focus on the Helmholtz resonator.

2.2 Control Methods

Several methods of noise control are available for mitigating acoustic excitation, some of which have been discussed for the control of flow-excited oscillations. Typical noise control methods are either active, passive, or hybrid techniques. Active methods generally use a secondary acoustic source to output an out-of-phase signal to destructively interfere with the incident acoustic field. This requires sensors to analyze the incident acoustic waveforms, a control system for analysis and generation of an out-of-phase signal, and an actuator to output the destructive signal. Active control is robust as it can be used to reduce the incident acoustic excitation for changing frequencies. This adaptability is advantageous for damping noise in systems with changing operating points or broadband acoustic excitation. Active methods can also be used to dampen acoustic wave generation from flow instabilities. However, active control requires several components and can therefore be quite intensive and expensive. Additionally, an improperly tuned active control system can actually increase the amplitudes of acoustic excitation [28].

Passive methods, on the other hand, simply rely on their material or geometric properties to reduce the amplitudes of acoustic excitation. They are therefore 'passive' in that they do not require energy to be input into the system to achieve damping. For damping noise in pipeline systems, various devices have been investigated in the literature. Absorptive liners, for example, dissipate some of the acoustic energy in ducts via the transfer of acoustic to thermal energy as the acoustic waves propagate through a material [29]. These materials are suitable for acoustic insulation, but also induce high pressure drops in pipeline systems. Other devices, such as the quarter wave resonator [30, 31], are reactive; they create reflections and destructive interference between incident and reflected waves at targeted frequencies. A quarter wave resonator can be attached to a pipeline or duct of interest as a sidebranch, whereby the reflections at its closed end result in resonance and absorption of energy from the main pipeline. However, quarter wave resonators may be excessively long if they are designed to target low frequencies.

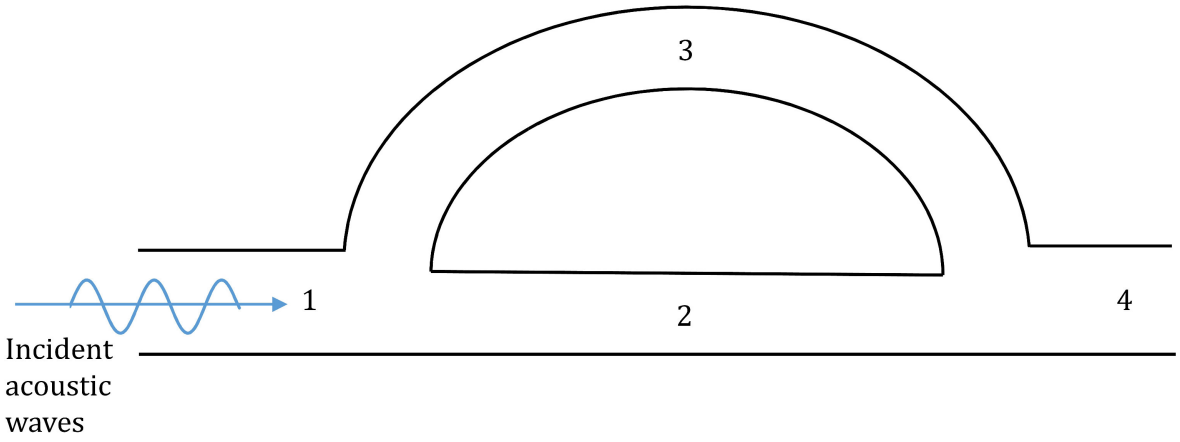

Figure 2.7: Schematic of Herschel-Quincke tube.

Another passive damping device that has been studied in some depth is the Hershel-Quincke (HQ) tube [32, 33]. The HQ tube is a parallel connection of two tubes, as shown in Figure 2.7. As the incident acoustic waves propagate from left to right through segment 1, they encounter the upstream junction of the HQ tube, and must propagate into both segments 2 and 3. The acoustic waves recombine at the downstream junction and subsequently propagate through segment 4. Since there is a difference in path lengths between segments 2 and 3, the recombined waves will destructively interfere for the frequencies that are out-of-phase. Additionally, the acoustic waves are reflected at both the upstream and downstream junctions because of changes in cross-sectional area, resulting in additional frequencies that are damped, as noted by Stewart [34]. More recently, Lato and Mohany [35] have shown that an HQ connected to a resonant system acts as a sidebranch resonator, whereby energy from the main pipeline is absorbed via resonance in the sidebranch (i.e. segment 3).

The Helmholtz resonator (HR) is another passive damping device that has been studied [36, 37, 38] because of its simplicity and relatively small size. The HR consists of an enclosed volume with a protruding neck that connects it to a system of interest. For attenuation of plane waves propagating in a pipe, the HR is connected to the pipeline

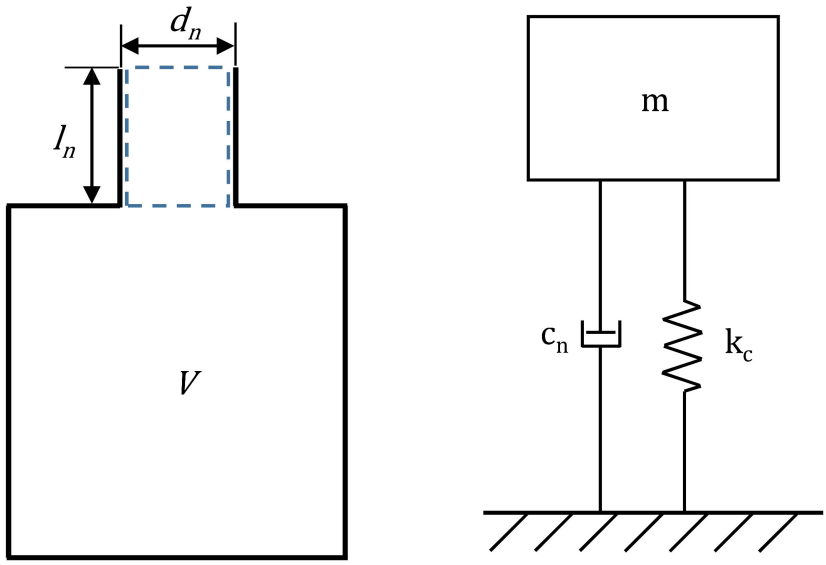

(a) (b)

Figure 2.8: Schematics of (a) a Helmholtz resonator and (b) the analagous structural vibration absorber.

as a sidebranch via its neck. A well-known classical, or lumped-parameter, approach is typically used to explain the behaviour of an HR in such a system. This approach is valid as long as the dimensions of the HR are small relative to the wavelength of interest [1]. According to the lumped parameter model, as acoustic waves pass over the opening of the neck, the mass of fluid in the neck oscillates and the fluid in the cavity volume acts as a stiffness, compressing and rarefying. This concept is shown in Figure 2.8, which shows (a) a schematic of a Helmholtz resonator and (b) its analagous structural vibration absorber. If the frequency of the acoustic excitation in the pipeline corresponds to the natural frequency of the HR, the HR resonates and some of the acoustic energy in the pipe is transferred to the resonator. Damping in the HR exists in the form of viscothermal and radiation losses at the neck, as well as jet-flows at the neck at high acoustic pressure amplitudes [39].

Using the lumped parameter model, the mass of air in the neck is defined as:

$$m = \rho A_n l_n \tag{2.2}$$

where ρ is the fluid density, A_n is the cross-sectional area of the neck, and l_n is the neck length. Early experiments revealed that the mass of fluid in the neck is larger than the physical neck length due to the entrainment of fluid as the fluid in the neck oscillates; some of the fluid on either side of the neck oscillates with the fluid in the neck. An effective neck length was suggested, which can be calculated using:

$$l_{eff} = l_n + \alpha \tag{2.3}$$

where α is the end correction value. For an HR neck with a circular cross-section, Kinsler et al. [1] suggested an end correction of $\alpha = 1.7r_n$, where r_n is the neck radius. The stiffness of the fluid in the cavity is defined as [40]:

$$k_c = \frac{\rho c^2 A_n^2}{V_c} \tag{2.4}$$

where c is the speed of sound and V_c is the volume of the cavity. Since the natural frequency of a dynamic vibration absorber is given by $\omega = \sqrt{k/m}$, the natural frequency of a Helmholtz resonator can therefore be expressed as:

$$f_{HR} = \frac{c}{2\pi}\sqrt{\frac{A_n}{V_c l_{eff}}} \tag{2.5}$$

It can be seen from Equation 2.5 that the cavity volume and neck dimensions can be selected in order to obtain a desired natural frequency of the Helmholz resonator. Since by analogy it behaves as a vibration absorber, a sidebranch HR will yield maximum acoustic attenuation when the excitation frequency in the pipeline is equal to the natural frequency of the HR. An HR will attenuate noise over a narrow bandwidth, with its natural frequency at the peak of the band, which is why HRs are typically used to attenuate tonal noise.

A large body of research has been devoted to accurately predicting the resonant frequencies of HRs. Different end correction values have been investigated by Ingard [41], who used the lumped-parameter analogy to theoretically determine α values based on the neck and cavity volume geometries. Alster [42] noted that no linear dimension of the HR should exceed a quarter wavelength of its resonant frequency, to prevent the formation of standing waves within the resonator. A revised form of the resonant frequency equation was provided, which is based on particle motion inside the neck and cavity volume for various geometries. Chanaud [43] developed an equation for the resonant frequency of an HR with rectangular volume and various neck geometries. Panton and Miller [44] formulated a revised resonant frequency equation for a cylindrical HR, which yields more accurate results for relatively longer resonator lengths.

Additionally, some work has focused on predicting the transmission loss (TL) of Helmholtz resonators, such as that by Selamet et al. [45]. A theoretical equation for the TL was developed, which is based on the resonator geometry and pipeline cross-sectional area, i.e.

$$TL = 10log_{10}\Big[1 + \Big(\frac{A_n}{2A_p}\frac{tan(kl_n) + (A_v/A_n)tan(kl_v)}{1 - (A_v/A_n)tan(kl_n)tan(kl_v)}\Big)^2\Big] \tag{2.6}$$

where A_n, A_v, and A_p are the neck, volume, and pipeline cross-sectional areas, respectively. l_c and l_v are the neck and volume lengths, respectively, and k is the wavenumber. This equation assumes planar wave propagation and neglects viscous effects. The theoretical TL obtained from the equation was subsequently compared to a 2-D analytical model and a 3-D boundary element method by Selamet et al. [40]. A sample of their results is shown in Figure 2.9, which shows a comparison of the transmission loss spectra of an HR for the various methods. It is observed that the theoretical equations and numerical simulation yield higher TL peak frequencies than the experimental result. Moreover, the amplitude of the TL peak for the theoretical and computational methods is significantly higher than the experimental results. This was attributed to the neglect of viscothermal

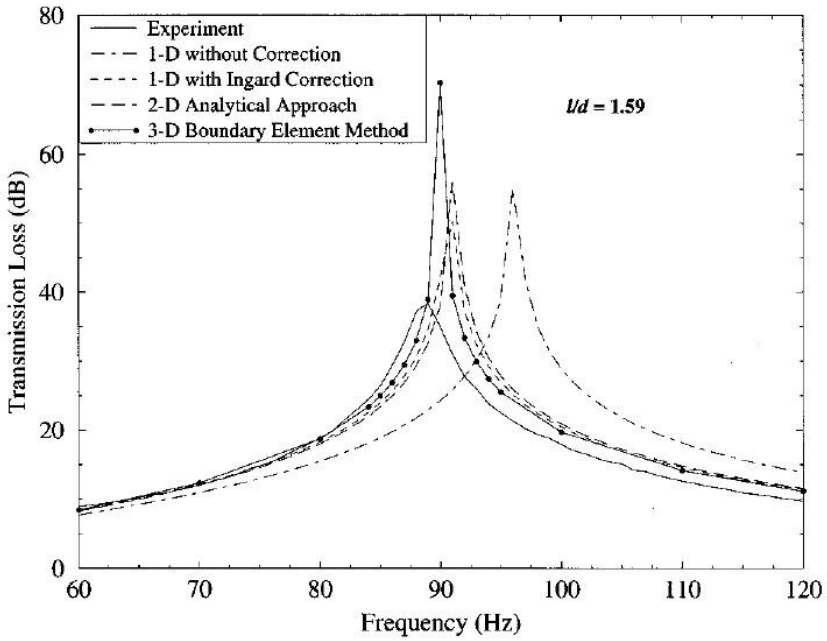

Figure 2.9: Transmission loss spectra of a single HR, obtained experimentally or using various analytical methods. Figure courtesy of Selamet et al. [40].

effects for the analytical methods used.

The effects of mean flow on the acoustic response of an HR have been studied from two main perspectives. The first comprises the field of research concerned with flow-excited Helmholtz resonators [46, 47, 48]. The mechanism of a flow-excited HR is similar to the fluid-resonant mechanism discussed above. A mean flow will result in an unstable shear layer over the neck opening of the HR. If the frequency of shear layer oscillations matches the natural frequency of the HR, the HR will resonate and generate sound. While this research provides interesting insights into the fluid mechanics of a flow-excited Helmholtz resonator, it does not directly address the effects of flow on the HR as an acoustic damping device.

The effects of mean flow on the acoustic attenuation achieved by an HR have also been considered to some extent in the literature. Anderson [49] experimentally investigated the effect of air flow on a single HR connected to a circular duct. It was found that the

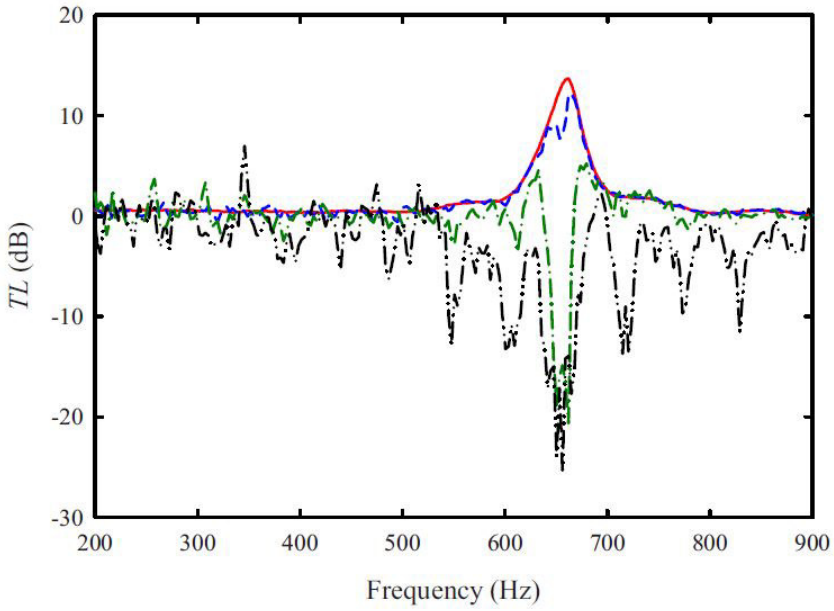

Figure 2.10: Transmission loss spectra of a single HR with various flow velocities. Red = 0m/s; Blue = 8 m/s; Green = 12 m/s; Black = 18 m/s. Figure courtesy of Tang [50].

presence of mean flow in the same direction as acoustic wave propagation results in an increase in the HR's natural frequency. This effect was considered to be caused by the end correction of the neck being 'blown away', resulting in a decrease in the effective neck length and a corresponding increase in resonant frequency, as can be seen from Equation 2.5. Tang [50] investigated the effect of low Mach number flow on the transmission loss of a ducted HR, as shown in Figure 2.10. It can be seen that the TL decreases with increasing flow velocities, and a negative TL (i.e. sound amplification) is observed with mean flow velocities greater than 10 m/s. However, it was noted that the shear layer oscillation frequencies for the neck dimensions studied did not correspond to the natural frequency of the HR, suggesting that this behaviour is not related to the flow-excited mechanism. The reasons for this behaviour were left to further investigation.

More recently, research has been devoted to the use of multiple HRs in pipeline or duct systems. Because a single HR will yield a high TL at its resonant frequency, Wang and Mak [51] considered the use of multiple sidebranch HRs to improve the bandwidth

of attenuation. It was found that the use of multiple HRs with constant periodic spacing (i.e. along the pipe axis) improves the noise attenuation band and amplitude. Wang and Mak [52] subsequently considered the effects of 'disorder' in a periodic HR array, either by using multiple identical HRs with different periodic distances between them, or by using HRs with different geometries (and consequently different resonant frequencies) and constant periodic spacing. It was found that the use of identical HRs with different periodic spacing results in discrete drops in the TL, as shown in Figure 2.11, suggesting that variance in the periodic spacing between multiple HRs is not advantageous for improving the amplitudes or bandwidths of attenuation. On the other hand, Figure 2.12 shows that the use of HRs tuned for different frequencies with constant periodic spacing improves the bandwidth of attenuation, while maintaining the discrete peak TLs of the individual resonators. Cai et al. [53] considered the use of multiple HRs mounted in the both the longitudinal (axial) and transverse directions. It was found that utilizing multiple HRs in the transverse directions in addition to those with uniform periodic spacing results in a broader noise attenuation band, without effects on the resonant frequency.

Cai et al. [54] also studied the use of multiple HRs by considering their energy storage, or noise attenuation, capacity. The area under the transmission loss curve can be viewed as the amount of acoustic energy transferred to the HR(s) from the pipeline system, i.e. the energy storage capacity. The theoretical and numerical study found that the periodic spacing between multiple HRs affects the bandwidth, peak frequency, and peak magnitude of attenuation, but not the area under the TL curve. In other words, the periodic spacing will change the spectral response of an HR system, but not the total energy absorbed by the HRs. Based on this finding, a 'noise control zone' was presented, as shown in Figure 2.13, which outlines the possible spectral distribution of TL that can be achieved by varying the periodic spacing between HRs.

The foregoing discussion of the literature shows that several aspects regarding the

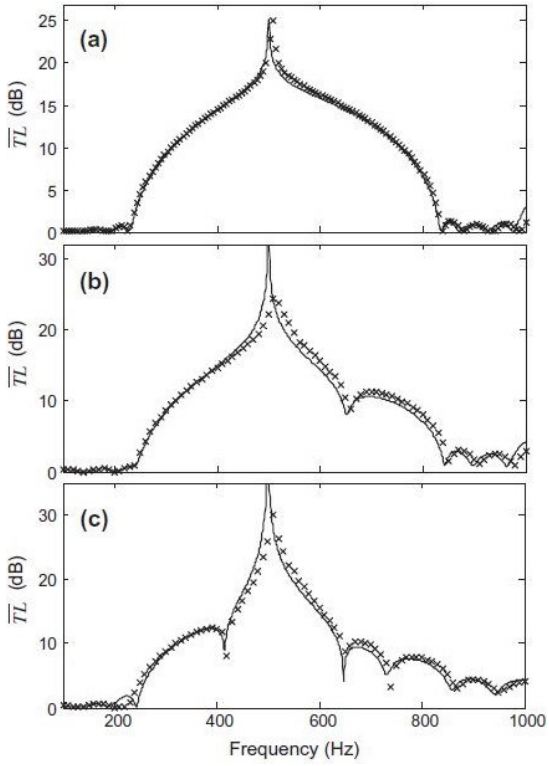

Figure 2.11: Average TL for five identical HRs with (a) uniform spacing, (b) spacing between first two HRs varied, and (c) spacing between the first three HRs varied. Figure courtesy of Wang and Mak [52].

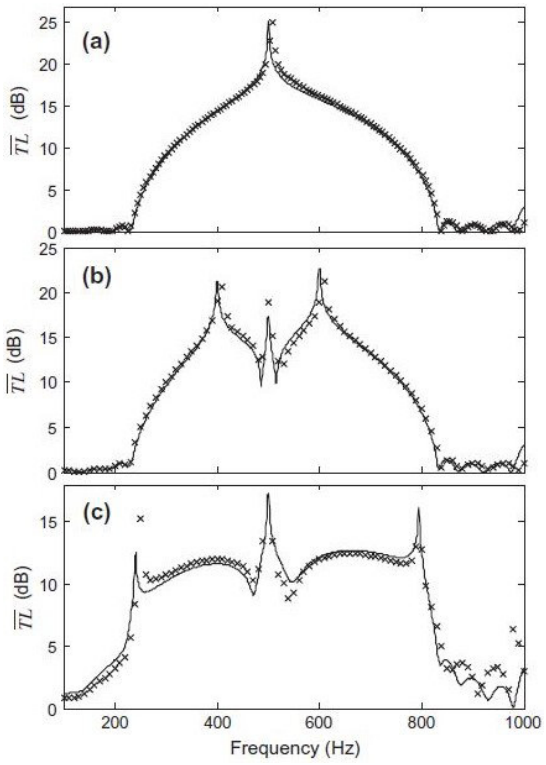

Figure 2.12: Average TL for five HRs with uniform spacing, for HRs with (a) the same resonant frequency, (b) shifting the first two resonators by 100 Hz, and (c) shifting the first two resonators to 250 Hz and 800 Hz, respectively. Figure courtesy of Wang and Mak [52].

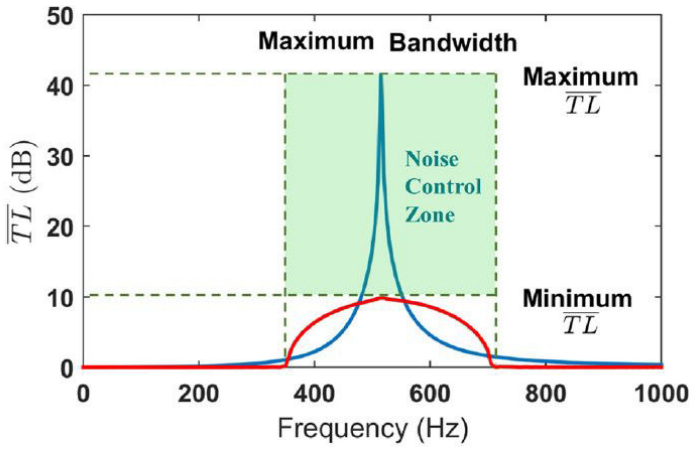

Figure 2.13: Noise control zone showing average TL vs. frequency for a ducted HR system. Figure courtesy of Cai et al. [54].

use of Helmholtz resonators as acoustic damping devices have been studied. However, the effects of certain parameters on the acoustic attenuation achieved by HRs should be investigated to ensure effective performance within a system of interest. For example, the relative size of the HRs to the pipeline should be considered to determine the required scaling of an HR. Although multiple HRs have been studied, the use of multiple, small-volume HRs to achieve levels of damping comparable to a single, large-volume HR has not been previously investigated. This may be of use for systems that have spatial limitations on the installation of HRs. The effect of location on the insertion loss should be investigated for both acoustically resonant and off-resonant cases, as the axial location may affect the performance of an HR. Hitherto, most research has focused on the transmission loss of an HR, which does not quantify the actual reduction in acoustic excitation within a given system caused by the insertion of a damping device. Mean flow velocities should be considered to clarify the effects of low Mach number flows on the attenuation achieved by HRs, since there have been discrepancies in the literature regarding this point.

2.3 Summary and Research Needs

The literature review highlights the significance and causes of acoustic pressure pulsations in pipeline systems, as well as methods that have been considered for their mitigation. For the attenuation of discrete excitation, as is desired for damping excitation of the blade passing frequency in industrial systems, the use of Helmholtz resonators is promising because of their narrow-band response, geometric simplicity, and relatively small size. However, the incorporation of damping devices in industrial systems requires a thorough understanding of their effects on the pipeline. This includes an understanding of the effects of an HR on a system's acoustic response, considering the effects of relative size and mean flows. A summary of aspects that require clarification is summarized as follows:

- The effects of HR cavity volume and pipeline diameter should be investigated to determine the required HR size to achieve significant damping for a given pipeline size.

- The effects of HR axial location for both resonant and off-resonant pipelines needs to be characterized to determine the sensitivity of the acoustic attenuation to location.

- The use of multiple HRs in various configurations should be studied to determine the arrangements that maximize acoustic damping for a discrete frequency of interest. Additionally, the use of multiple, relatively small HRs is considered to determine if the achieved damping is comparable to that of a single, large-volume HR.

- Both the magnitude and directionality of mean flows should be considered to determine the sensitivity of an HR's acoustic attenuation to mean flow.

- The mechanism of attenuation of a sidebranch HR should be clarified to explain the behaviour of an HR as an acoustic damping device.

- The effect of incident pressure amplitude on the transmission loss of an HR should be studied, to determine the scalability of HRs from a test setup to the system of intended application. This will also clarify the 'source independence' of transmission loss as a measurement technique.

Chapter 3

Experimental Setup and Methodology

To fulfill the objectives of this work, an open loop pipeline setup was designed and constructed to allow for the evaluation of various damping devices. The experimental work is comprised of three main stages. In the first, the acoustic damping of Helmholtz resonators is evaluated using both transmission loss and insertion loss measurements. The effects of HR and pipeline volume, axial location, multiple devices, and mean flow are considered. The second stage is primarily concerned with explaining the trends seen in the first; the mechanism of attenuation of the HR is considered to help provide insights into the reasons for the effects of various parameters on the acoustic damping achieved. In this second stage, pressure and phase measurements are taken, including those necessary to determine the reflection coefficient. In the third stage, the effects of acoustic excitation amplitude on the acoustic damping of an HR is investigated. The following sections provide a description of the experimental setup and the methodology used for analysis.

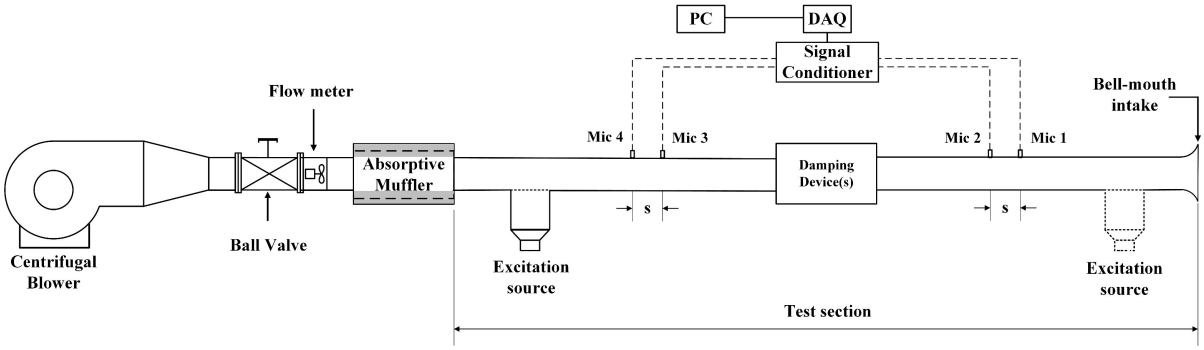

Figure 3.1: Schematic of experimental setup for 4 inch diameter pipeline and mean flow.

3.1 Experimental Setup

An experimental setup was constructed to allow for the evaluation of various damping devices and flow rates. A schematic of the setup is shown in Figure 3.1. The frequency of interest is 150 Hz, and the setup parameters were selected so that the damping devices could be accurately evaluated at this frequency. The setup consists of an open loop air pipeline with a main test section diameter of 4 inches. For this diameter, the cut-off frequency is nearly 2000 Hz [2], which means that plane wave propagation can be considered for the frequency range of interest. A centrifugal blower drives the mean flow, and a ball valve and flow meter are used to control and measure the flow velocities in the test section, respectively. An absorptive muffler is used to mimic an open end and isolate the test section from the noise emitted by the blower and valve. The test section has a bellmouth at its inlet to reduce the turbulence and pressure drop. The length of the test section can be adjusted for resonance (i.e. standing wave) and off-resonance (i.e. travelling wave) cases. For resonance, its length is approximately 5.3 m, which is selected to excite the fifth longitudinal acoustic mode of the 150 Hz frequency. The sound pressure level (SPL) with 150 Hz excitation in the resonant test pipe was 150 dB. For

off-resonance experiments, its length was changed to approximately 5 m, so that 150 Hz is one of the system's antiresonant frequencies. Pipe diameters of 2 and 6 inches were also utilized to determine the effects of relative pipeline size, as shown in the following chapter (see Figure 4.3. However, for all other experiments discussed, the measurements were taken in the 4 inch diameter piping.

The excitation source is connected to the test section via a 'T' connection and is capable of providing either broadband excitation or discrete frequency pulses. The amplitude of the source excitation is controlled using an amplifier. The source consists of a loudspeaker with a back enclosure that is acoustically insulated, ensuring that the excitation is provided directly into the pipeline and eliminating flanking noise transmission. It is connected to the test section either near the inlet or the muffler, as shown in Figure 3.1. This is required for the two source-location method [55] for determining a damping device's transmission loss, which will be discussed later in this section. It also allows for the evaluation of damping devices with mean flows in the same or opposite directions to acoustic wave propagation.

For the evaluation of the acoustic damping achieved by various HR configurations, 1/4" diameter pressure microphones are flush-mounted to the inside of the pipe to measure the acoustic pressures in the test section. The microphones were calibrated using a sound calibrator with a known reference frequency and excitation level. For the measurement of acoustic pressure inside the cavity volume of an HR, the pressure microphone is flush-mounted to the inside of the cavity. The raw signals from the microphones pass through a signal conditioner and are then digitized by the data acquisition (DAQ) card. The digital signal is processed and recorded for analysis. The software used for data acquisition also generates the acoustic signals for the excitation source, so that the measurements and acoustic excitation are synchronized. For the experiments discussed in this thesis, the microphone signals were recorded using sampling rate of 20 kHz for 90 seconds. For each set of experiments, ensemble averaging was performed using 90

ensembles to obtain a frequency resolution of 1 Hz.

3.2 Transmission Loss Measurements

The transmission loss (TL) of a damping device is a ratio of the incident to transmitted acoustic power of the device [56], expressed on a logarithmic scale, i.e.

$$TL = 10 \log_{10} \frac{W_i}{W_t} \tag{3.1}$$

where W_i and W_t are the incident and transmitted acoustic power, respectively. Transmission loss measurements are useful for quantifying the attenuation of a damping device independently of system parameters such as the pipeline end terminations. TL is also often cited as being independent of the acoustic source. It is therefore a useful tool for performing spectral analyses and determining the relative magnitudes of acoustic attenuation of damping devices. The TL measurements discussed in this thesis were performed with broadband excitation from the source, in order to ensure that the damping devices are tuned to target the 150 Hz frequency of interest and obtain a quantitative measure of damping device performance.

The two source-location method described by Munjal and Doige [55] is used for transmission loss measurements. This method is used to determine the transfer matrix of an acoustic element, from which the TL is calculated. The transfer matrix relates the acoustic pressures and velocities acoustically upstream of an acoustic element to those downstream of the element, as shown in Figure 3.2. This is shown mathematically using:

$$\begin{bmatrix} p_n \\ v_n \end{bmatrix} = \begin{bmatrix} T_{11} & T_{12} \\ T_{12} & T_{22} \end{bmatrix} \begin{bmatrix} p_{n+1} \\ v_{n+1} \end{bmatrix} \tag{3.2}$$

where p is the acoustic pressure, v is the acoustic particle velocity, and the subscripts n and $n+1$ denote the upstream and downstream locations, respectively. T_{11}, T_{12}, T_{21}, and

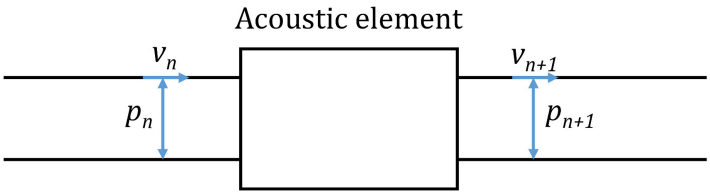

Figure 3.2: Schematic of general representation of acoustic element for the transfer matrix method.

T_{22} are the coefficients, or four poles, that comprise the transfer matrix and are complex functions of the frequency. If the transfer matrices of adjacent acoustic elements are known, they can be multiplied in order to determine the overall transfer matrix of the 'total' acoustic element.

In order to determine the transfer matrix of any acoustic element using this method, microphone measurements at four locations are required. While it is possible to use fewer than four microphones, this necessitates moving the microphone(s) to the four required locations for each set of experiments, increasing the required time and introducing additional error. Therefore, four microphones were used. Two are placed upstream and two downstream of the element, as shown in Figure 3.1, which allows for the determination of acoustic pressure and velocity on either side of the element. The microphones in each pair are separated by spacing s, as shown in the figure. The microphone spacing is chosen in order to maximize the accuracy over the frequency range of interest, considering that larger spacing enhances accuracy, but also that $s \leq 0.8c/2f_u$, where c is the speed of sound and f_u is the upper frequency limit (ASTM E2611 [2]). For the spacing used, the upper frequency limit is approximately 860 Hz, which is sufficiently high considering the frequency of interest is 150 Hz.

For the test section with the microphone locations shown, the acoustic pressures and

particle velocities at locations 1 and 4 can be related using:

$$\begin{bmatrix} p_{1,a} \\ v_{1,a} \end{bmatrix} = \begin{bmatrix} T_{11,12} & T_{12,12} \\ T_{21,12} & T_{22,12} \end{bmatrix} \begin{bmatrix} T_{11,23} & T_{12,23} \\ T_{21,23} & T_{22,23} \end{bmatrix} \begin{bmatrix} T_{11,34} & T_{12,34} \\ T_{21,34} & T_{22,34} \end{bmatrix} \begin{bmatrix} p_{4,a} \\ v_{4,a} \end{bmatrix} \tag{3.3}$$

where $p_{i,a}$ and $v_{i,a}$ are the acoustic pressures and particle velocities, respectively, at point i, and a denotes the configuration with the speaker at the inlet. $T_{11,jk}$, $T_{12,jk}$, $T_{21,jk}$, and $T_{22,jk}$ are the transfer matrix coefficients for the acoustic element between points j and k. It should be noted that the transfer matrices between points 1 and 2 as well as points 3 and 4 are known from theory, since these are the transfer matrices of a straight pipe section. The four poles of a straight pipe are simply functions of the frequency, length of pipe, speed of sound, fluid density, and mean flow velocity (if applicable). Since the pressures and particle velocities are measured quantities, it can be seen from Equation 3.3 that there are four unknowns, i.e. the transfer matrix coefficients for the acoustic element between points 2 and 3, but only two equations. The source is moved to the muffler, which is referred to as configuration b, and two additional equations are obtained:

$$\begin{bmatrix} p_{4,b} \\ v_{4,b} \end{bmatrix} = \frac{1}{\Delta_{12}} \begin{bmatrix} T_{11,12} & T_{12,12} \\ T_{21,12} & T_{22,12} \end{bmatrix} \frac{1}{\Delta_{23}} \begin{bmatrix} T_{11,23} & T_{12,23} \\ T_{21,23} & T_{22,23} \end{bmatrix} \frac{1}{\Delta_{34}} \begin{bmatrix} T_{11,34} & T_{12,34} \\ T_{21,34} & T_{22,34} \end{bmatrix} \begin{bmatrix} p_{1,b} \\ v_{1,b} \end{bmatrix} \tag{3.4}$$

where Δ_{jk} is the determinant of the transfer matrix jk, i.e. $\Delta_{jk} = T_{11,jk}T_{22,jk} - T_{12,jk}T_{21,jk}$. Using Equations 3.3 and 3.4, the four equations can be solved; the four poles for element 2-3 can be evaluated. From these four poles, the transmission loss can be calculated using:

$$TL = 20 \log_{10} \frac{1}{2} \left| T_{11,23} + \frac{T_{12,23}}{\rho c} + \rho c \cdot T_{21,23} + T_{22,23} \right| \tag{3.5}$$

In order to baseline the transmission loss measurements using the two source-location method, an expansion chamber (reactive muffler) was constructed and tested. An expansion chamber simply consists of an expansion in diameter from the main pipe, and relies on destructive interference between incident and reflected acoustic waves within the

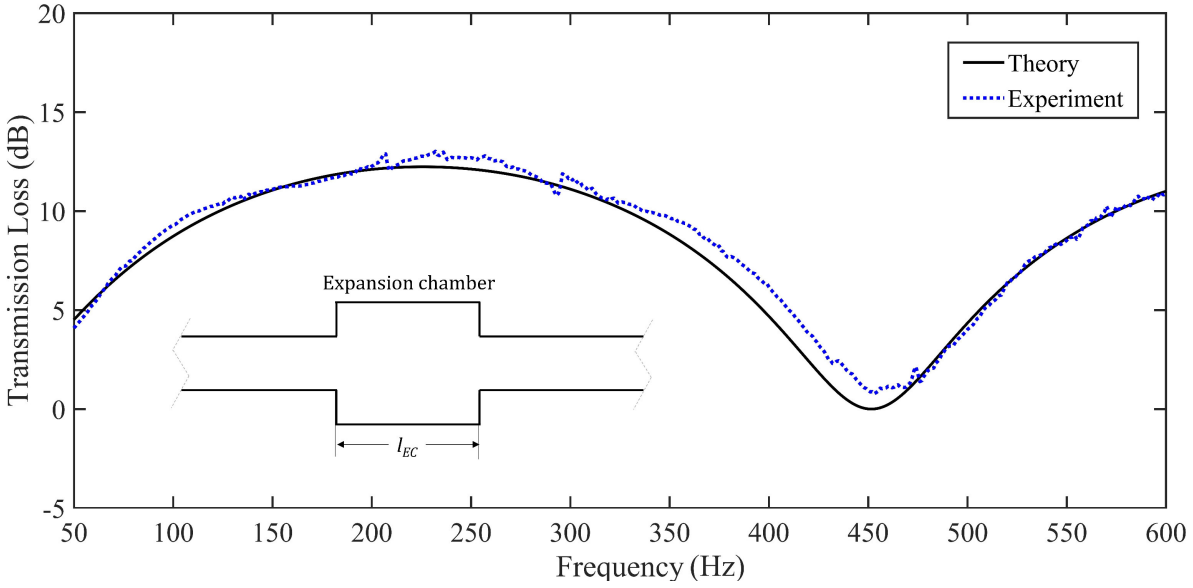

Figure 3.3: Theoretical and experimental transmission loss of an expansion chamber.

chamber to dampen acoustic excitation. An expansion chamber has known theoretical TL values [57], which are calculated according to:

$$TL_{EC} = 10\log_{10}\left[1 + \frac{1}{4}\left(h - \frac{1}{h}\right)^2 sin^2(kl_{EC})\right] \tag{3.6}$$

where h is the ratio of cross-sectional areas between the main pipe and the expansion chamber, k is the wavenumber, and l_{EC} is the length of the expansion chamber. The results for transmission loss measurements for the expansion chamber are shown in Figure 3.3. It can be seen that there is very good agreement between the experimental and theoretical TL values over a large frequency range.

3.3 Insertion Loss Measurements

Insertion loss (IL) measurements quantify the actual reduction in sound in a given system caused by the insertion of a damping device. IL is therefore often cited as giving a 'true measure' [58] of damping device performance. The IL is obtained by taking acoustic

pressure measurements in the test section before and then after a damping device is inserted. Measurements must be taken acoustically downstream of the damping device location; the device must be inserted between the acoustic source and the measurement location. The difference in sound pressure level between the two cases is known as the insertion loss [59]:

$$IL = SPL_1 - SPL_2 \tag{3.7}$$

where 1 and 2 denote measurements in the system before and after the damping device is inserted, respectively. For the IL measurements discussed in this thesis, excitation from the source was provided in the form of discrete pulses at the 150 Hz frequency of interest. This was done in order to emulate the conditions in industry, whereby turbomachinery creates acoustic pressure pulsations at the blade passage frequency. The IL therefore gives a measure of the reduction in the 150 Hz excitation in a given test section.

The effect of microphone placement was investigated to determine the sensitivity of IL measurements to axial location. It was found that for low frequencies, including the 150 Hz frequency of interest, the IL is independent of microphone location (as long as the microphone is acoustically downstream of the damping device(s)). Moreover, while only one microphone is needed for the measurement of IL, two microphones were used, with the average of the two shown in the results.

3.4 Transfer Function and Reflection Coefficient Measurements

Transfer function measurements between microphone signals were taken for the comparison of pressure amplitude and phase for HRs connected to the system in various configurations. The transfer function is defined as:

$$H_{12} = \frac{p_1}{p_2} \tag{3.8}$$

where p is the complex-valued pressure at microphone locations 1 and 2. The transfer function is therefore a frequency-dependent value that represents the ratio of acoustic pressure amplitude and phase difference between the two locations. Transfer function measurements were corrected for phase mismatch according to ASTM E-1050 [60].

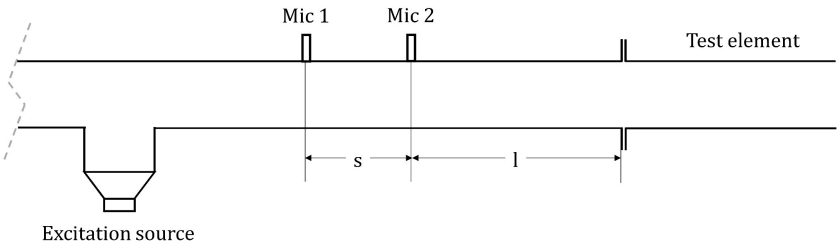

Figure 3.4: Schematic of microphone locations for reflection coefficient measurements.

The ratio of reflected to incident acoustic pressure is known as the reflection coefficient. The reflection coefficient for a test element of interest, as shown in Figure 3.4, can be found using the transfer function according to [62]:

$$R = \frac{H_{12} - e^{-iks}}{e^{iks} - H_{12}} e^{i2k(s+l)} \tag{3.9}$$

where k is the wavenumber, i.e. $k = \omega/c$, s is the microphone spacing, and l is the distance from the test element to the closest microphone (i.e. mic 2). In order to baseline these measurements, the reflection coefficient for an unflanged open end was measured and compared to the theoretical values provided by Levine and Schwinger [61]. The results are shown in Figure 3.5, which shows good agreement between experiment and theory.

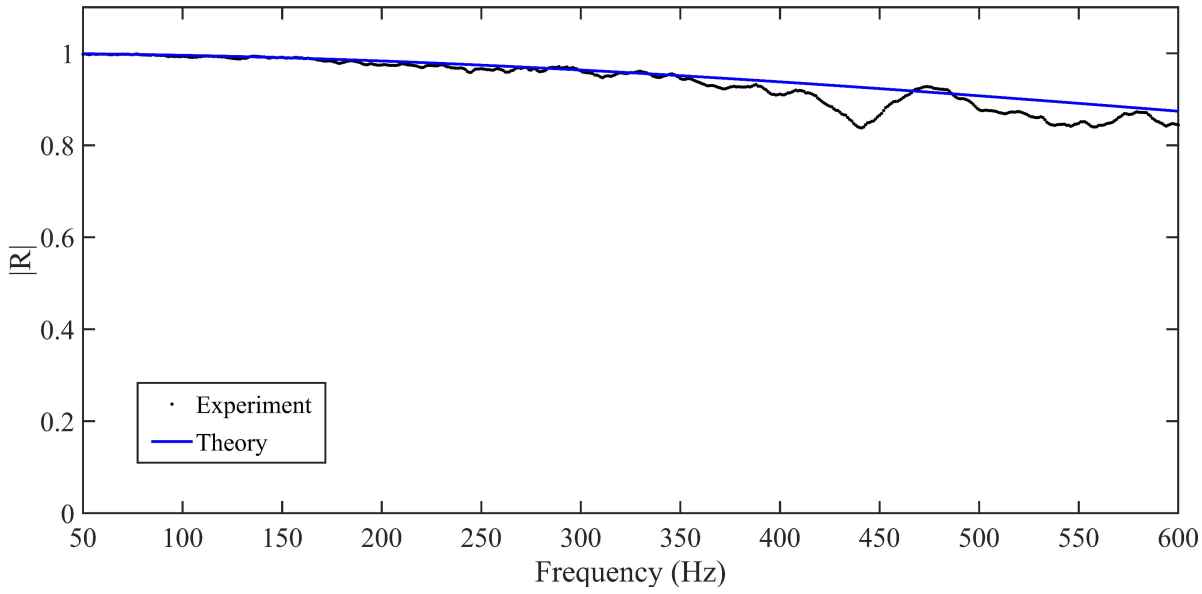

Figure 3.5: Theoretical [61] and experimental reflection coefficient for an open end termination.

3.5 Tested Helmholtz Resonators

Helmholtz resonators with various dimensions were constructed to target the 150 Hz frequency of interest. All of the tested HRs have cylindrical cavities with concentric cylindrical necks, which was selected for ease of construction. As Equation 2.5 shows, the resonant frequency of an HR is dependent upon its volume, neck length, and neck cross-sectional area. Accordingly, a change in HR cavity volume must be complemented with a change in neck parameters to maintain a particular resonant frequency. Schematics of the relative sizes of the tested HRs is shown in Figure 3.6. An overview of the dimensions of the HRs used is shown in Table 3.1. It can be seen that HRs with different cavity volumes were constructed with different neck lengths so that all of their resonant frequencies are 150 Hz. For ease of reference, the three HR sizes are referred to as the '1 L', '0.5 L', and '0.33 L' HRs, which is sufficiently representative of their relative volumes. The calculated resonant frequencies for each HR was calculated using the lumped-parameter method,

i.e. Equation 2.5, and is shown both before and after considering the end correction factor for the neck length. The end correction recommended by Kinsler et al. [1] was used, i.e. $\alpha = 1.7r_n$.

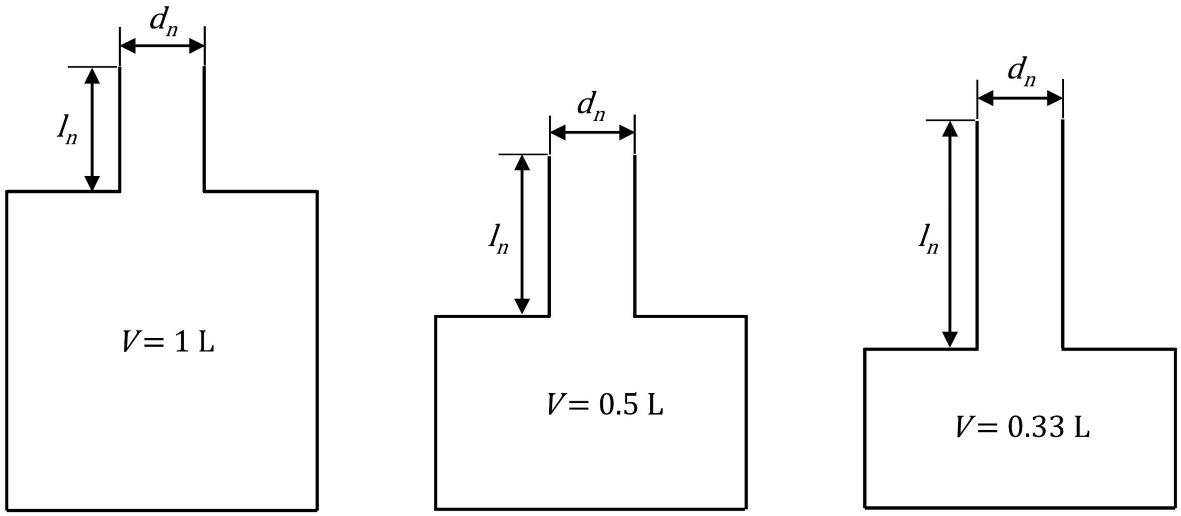

Figure 3.6: Schematic of tested HR sizes.

Table 3.1: Dimensions of the tested Helmholtz resonators.

HR dimensions	**1 L HR**	**0.5 L HR**	**0.33 L HR**
Neck diameter (cm)	2.7	2.7	2.7
Neck length (cm)	3.8	10.2	17.1
Cavity volume (L)	1.27	0.61	0.39
Relative volume (compared with 1 L HR)	1	0.48	0.31
Resonant frequency (Hz)	187.5	165.7	160.4
Resonant frequency w/ end correction (Hz)	148.1	149.7	150.6

Chapter 4

Acoustic Damping of Helmholtz Resonators

One of the primary objectives of this thesis is to investigate optimal configurations of HRs for damping low frequency excitation in industrial pipeline systems. Therefore, the effects of various parameters on the acoustic damping achieved using HRs was evaluated. Namely, the effects of HR cavity volume, axial location, and the use of multiple HRs was considered for both resonant and off-resonant test pipes. Mean flow velocity and directionality was also considered. This chapter presents the effects of these parameters on the acoustic damping achieved.

4.1 Effect of HR Volume

The effects of increasing the HR volume were investigated by evaluating the acoustic damping of HRs with 0.33 L, 0.5 L, and 1 L cavity volumes. The different HR volumes have varying neck lengths to ensure they all target the 150 Hz frequency of interest, as summarized in Table 3.1. It can be seen that an increase in cavity volume must be accompanied by a decrease in neck length to maintain the resonant frequency. No linear dimension of any HR exceeds a quarter wavelength of its resonant frequency, to prevent

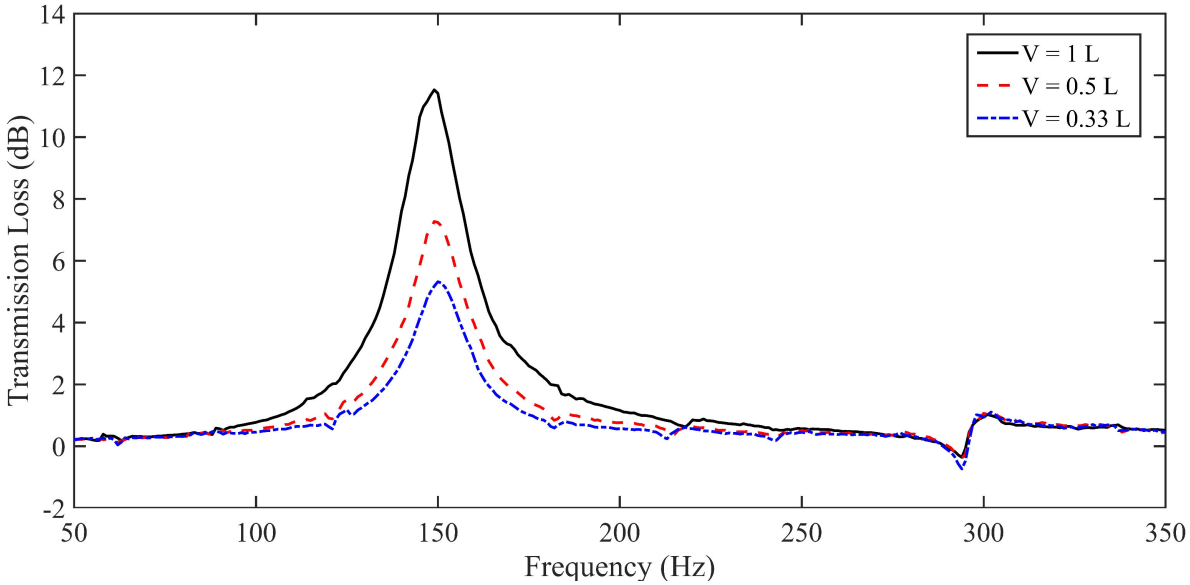

Figure 4.1: Transmission loss vs. frequency for various HR volumes.

the formation of standing waves.

HRs with various volumes were inserted into the resonant test pipe at an acoustic pressure antinode, and the TL was evaluated using the two source method described earlier. The results are shown in Figure 4.1. It can be seen that the peak TL for all HRs used is at 150 Hz, which shows that they are correctly tuned. The experimental resonance frequency therefore closely matches the theoretical resonance frequencies from Table 3.1, which were obtained using the end correction value presented by Kinsler et al. [1]. It is also seen that a larger cavity volume yields a higher transmission loss, with the 0.33 L, 0.5 L, and 1 L HRs achieving TLs of approximately 5 dB, 7 dB, and 12 dB, respectively. A maximal volume is therefore desirable for acoustic damping. However, in addition to the quarter wavelength restriction, there are practical limitations to the design and incorporation of large-volume HRs. For pipeline or duct systems where high levels of damping are necessary, a single, large-volume HR may be impractical because of size and access limitations. Additionally, the acoustic damping achieved by HRs may be sensitive to their relative placement along a piping system.

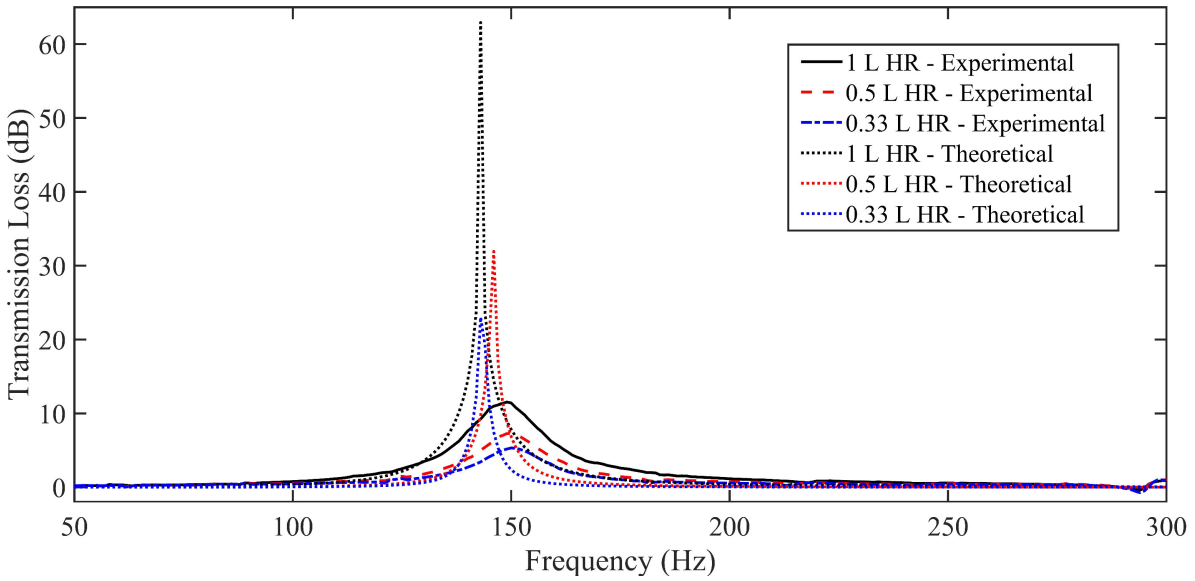

Figure 4.2: Theoretical [45] and experimental transmission loss for various HR sizes.

The experimental transmission loss curves for the various HR sizes was also compared to the theoretical TL shown in Equation 2.6 from Selamet et al. [45]. The results are shown in Figure 4.2, which show a significant variance between the theoretical and experimental TL spectra. First, it can be seen that the theoretical amplitudes of transmission loss are much higher than those obtained experimentally. For instance, the 1 L HR yields a TL of over 60 dB with the theoretical model, but only 12 dB was measured experimentally. This is attributed to the omission of damping considerations in the theoretical model. Second, the peak of the TL curve, which corresponds to the resonant frequency of the HR, is shifted to lower frequencies for the theory compared with experiment. While this shift is slight (at most 7 Hz), it deviates further from the actual resonant frequencies than the theoretical values obtained using the lumped-parameter model, as presented in Table 3.1. This is because the theory is more accurate for HRs with cavity volume lengths much larger than the cavity diameter [45], which is not the case here. Lastly, it is observed that the 'sharpness', or quality factor, of the TL curve is much lower for the experimental results than the theory. The theoretical transmission loss curves show

a sharp peak with very narrow bandwidth, whereas the experimental results yield much larger bands of attenuation with more rounded peaks. This effect is also attributed to the neglect of damping in the theory. This can be understood by considering the analogy between HRs and vibration absorbers. Compared to an undamped dynamic vibration absorber, a damped one will have lower oscillation magnitudes at its resonant frequency, but also a larger frequency band for which it is effective [63]. The theoretical curve can therefore be treated as the undamped case with narrow peaks of high magnitude, while the experimental curves, which are clearly affected by damping, show considerably lower peak values with larger bandwidths of attenuation.

The transmission loss measurements shown here for the resonant test pipe were identical to those obtained in the off-resonant test pipe. This finding agrees with theory, since the transfer matrix of an acoustic element is independent of its placement along the standing waves in a given experimental setup. In other words, TL measurements are independent of the system resonance. This shows the value of transmission loss as a measurement technique - it eliminates system-specifiic effects and gives a measure of the damping device itself. It also highlights the main limitation of TL as a measurement technique, since it does not represent the actual reduction in acoustic excitation achieved by inserting a device into a given system.

The effects of volume can also be considered by considering the effect of pipeline system diameter. Since the main test section diameter used was 4 inches, additional test sections of 2 and 6 inches were used to investigate the effect of pipeline size. The results are shown in Figure 4.3. It can be seen that for all HR sizes, the TL decreases with an increase in pipe diameter. The trend follows a curve whereby the attenuation seems to asymptotically approach a minimum value as the pipe diameter is increased, with larger HR values expectedly yielding higher TL values. This behaviour can be related to the relative size of the HR and its connection to the pipeline. Since all HRs used have a neck diameter of 1 inch, the increase in pipe diameter corresponds to a decrease in the

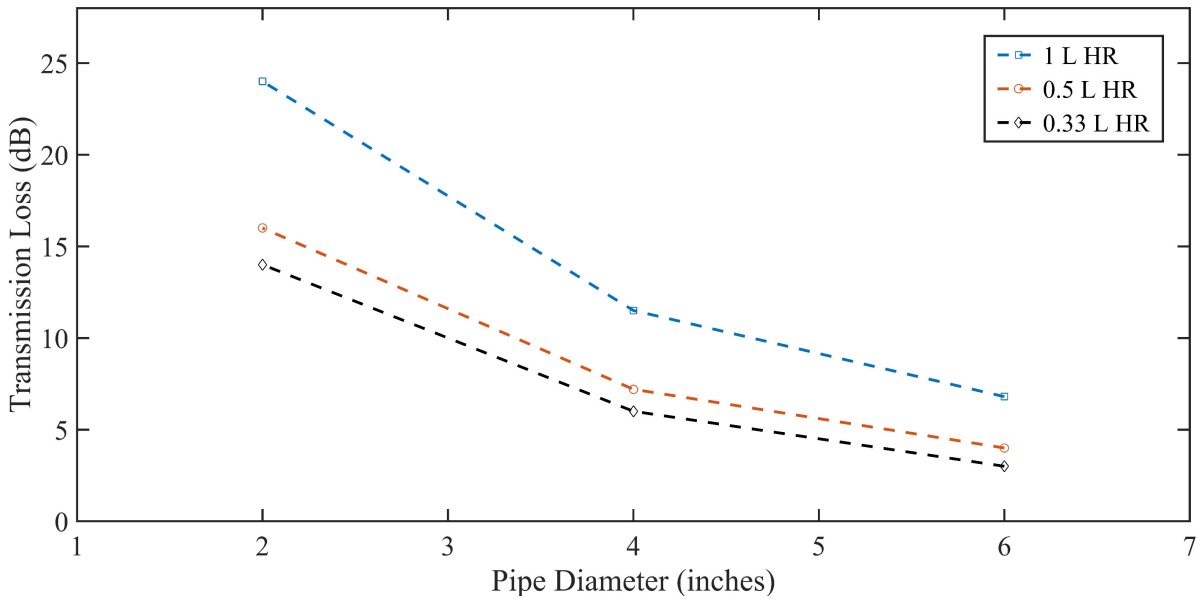

Figure 4.3: Transmission loss (peak values extracted at 150 Hz) for various HR volumes in different pipeline diameters.

relative size of the sidebranch connection. For example, the HR neck opening is half the diameter of the 2 inch pipe, but only one-sixth the diameter of the 6 inch pipe.

4.2 Effect of HR Location

In order to investigate the effect of HR location along a pipeline, a single HR was placed at multiple axial locations of a resonant and off-resonant test pipeline. As discussed above, transmission loss measurements are independent of location, so the insertion loss was evaluated to quantify the acoustic damping achieved at the various locations. The IL is sensitive to damping device location, and gives a true measure of damping device performance within a system of interest. First, the effect of location was considered for a resonant test pipe. Since the acoustic resonance in the test pipe manifests as a standing wave, the relative location of the HR to the acoustic pressure distribution of the standing wave can be used as a reference for its location, as shown in Figure 4.4(a).

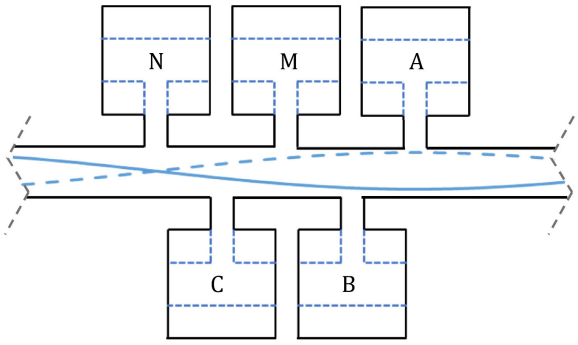

(a)

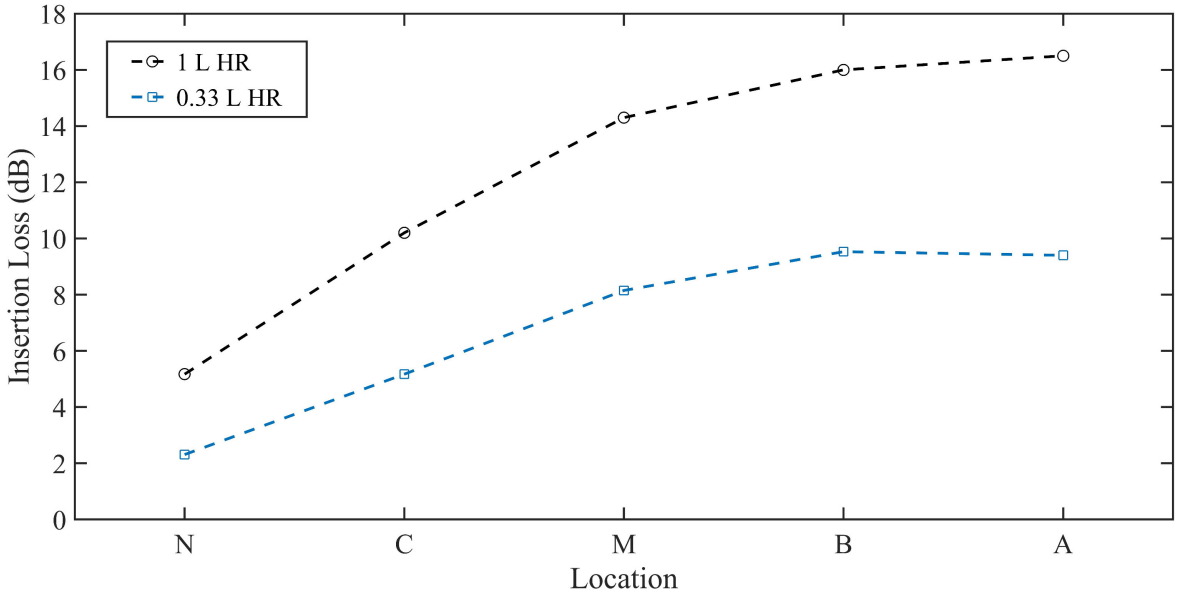

(b)

Figure 4.4: (a) Schematic of HR locations relative to acoustic standing wave, and (b) Insertion loss of 0.33 L and 1 L HR at various locations along standing wave.

Location 'N' corresponds to an acoustic pressure node, 'A' to an antinode, and 'M' to the midpoint between node and antinode. 'C' is located midway between 'N' and 'M', and 'B' is midway between 'M' and 'A'. The IL of a single 0.33 L or 1 L HR at these locations was obtained by measuring the reduction in SPL achieved with 150 Hz pulse excitation. The results are shown in Figure 4.4(b), which clearly shows that the acoustic damping is dependent upon the HR placement relative to the acoustic standing wave. Maximal damping is achieved at the acoustic pressure antinode and minimal damping is achieved at the node. It is interesting to note that the IL achieved by a 0.33 L HR close to an antinode is higher than that achieved by a 1 L HR at a node. This shows that small, well-placed devices can be used instead of relatively larger ones, which may be of use in applications where space limited or large devices are impractical. Therefore, although the TL is higher for larger-volume HRs, the actual damping achieved in a system is also highly dependent on its location. This shows the importance of insertion loss measurements and the significance of considering damping device location for a resonant system.

It should also be noted that the IL follows a curved trend, whereby it increases with decreasing slope as the HR is moved from the acoustic pressure node to the antinode. To verify this correlation between IL and location for a resonant system, a single 1 L HR was inserted at multiple locations along a full wavelength of the resonant test pipe, as shown in Figure 4.5. It can be seen that the IL follows the acoustic pressure distribution of the standing wave, with minimal IL at the nodes, and maximal attenuation at the antinodes. The insertion loss is therefore clearly related to the acoustic pressure distribution of the resonant test pipeline. The small variance between the IL maxima and the 'A' locations and between the IL minima and 'N' locations is caused by a slight shift between the theoretically determined and actual standing wave formation.

The reasons for this behaviour is attributed to how the HR affects the acoustics of the test pipe. As acoustic excitation at the resonant frequency of the HR passes over its neck, its neck fluid oscillates as the volume of fluid in its cavity compresses and rarefies.

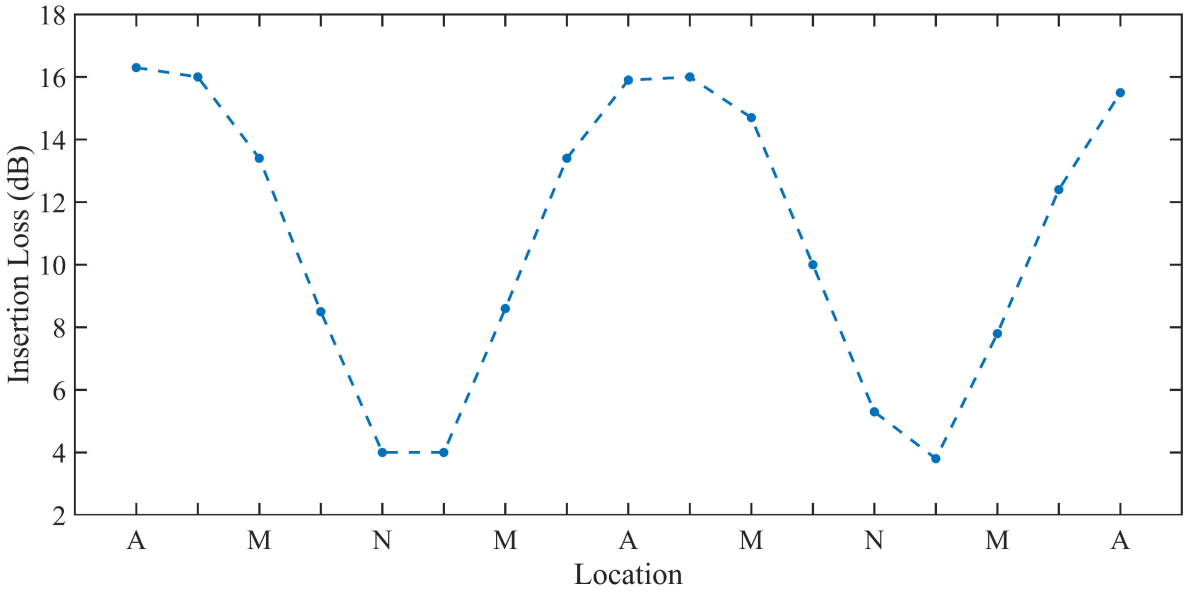

Figure 4.5: Insertion loss of a single 1 L HR at various locations along a resonant test pipe.

Therefore, at its junction with the pipeline, the HR acts as a location of maximum acoustic particle velocity, or mininum acoustic pressure. Accordingly, when the HR is inserted at an acoustic pressure node, i.e. an acoustic particle velocity antinode, of a resonant system, it achieves minimal damping because its location coincides with an existing minimum pressure location. The HR therefore does not disrupt the coupling that results in acoustic resonance in the main pipe, since at this location it does not effectively change the standing waveform in the main pipe. Converesely, when the HR is placed at an acoustic pressure antinode of a resonant system, it imposes a pressure minimum, disrupting the standing wave formation and consequently achieving maximal acoustic damping. Experimental measurements to clarify this mechanism are presented in the next chapter, which discusses the mechanism of attenuation of an HR.

The effect of HR location for an off-resonant test pipe was also considered by measuring the insertion loss of a single 1 L HR at various axial locations. The distance of the HR from the open end termination was used as a reference for the HR location since

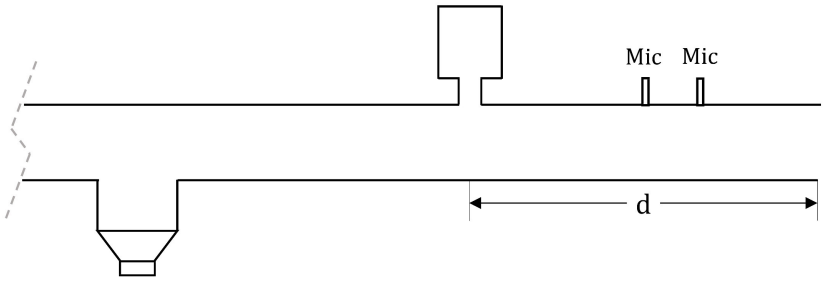

(a)

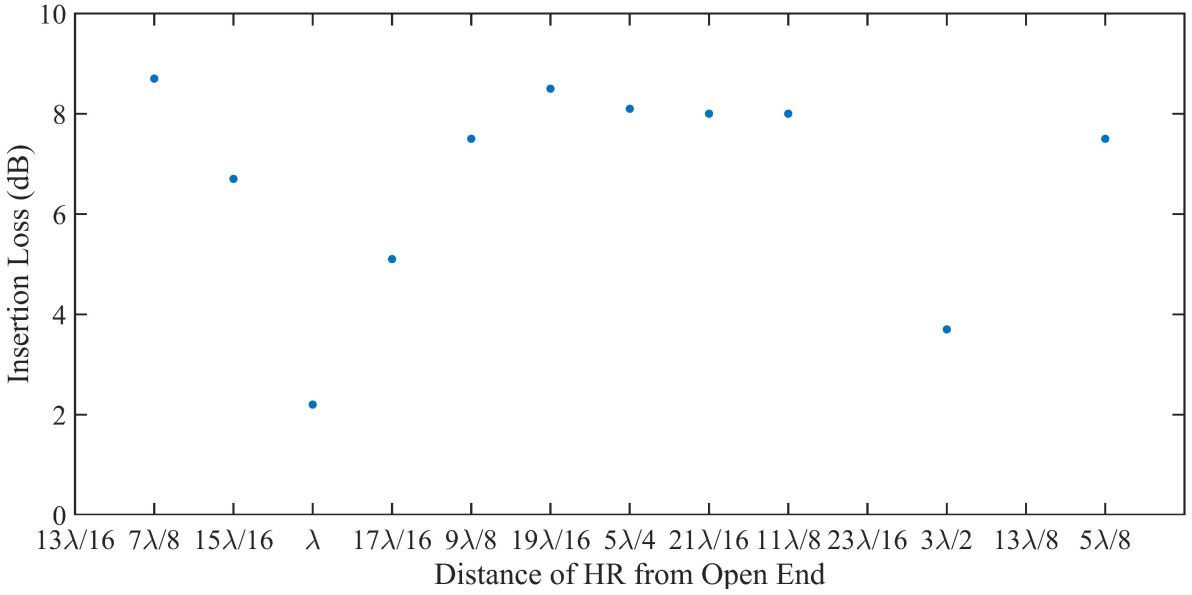

(b)

Figure 4.6: (a) Schematic of HR locations relative to open end for off-resonance IL measurements, and (b) Insertion loss of 1 L HR at various distances from open end.

there was no standing waveform in the off-resonant pipe, as shown in Figure 4.6(a). The IL for an HR at various distances, given in terms of wavelength of the 150 Hz frequency of interest, are shown in Figure 4.6(b). It can be seen that the IL at several locations is approximately 8 dB, with notable dips in the IL at $d = \lambda$ and $d = 3\lambda/2$, where the IL is 2.2 dB and 3.7 dB, respectively. The decreases in attenuation at these locations is caused by the behaviour described earlier, which is elucidated in the next chapter. The effects of axial location, in addition to the effects of HR volume discussed in the previous section, can both be considered for the use of multiple HRs. This is desirable in applications where high levels of damping are required or where characterizing the acoustics of a pipeline system is difficult.

4.3 Effects of Multiple HRs

While the use of multiple HRs has been considered in the literature [51, 52, 53, 54, 64], most of this work is concerned with improving the bandwidth of attenuation for targeting broadband noise. However, for targeting discrete excitation of high-amplitude and low frequency, it may be desirable to use multiple, relatively small devices instead of a single, large device. This is because the size of a device is limited by the quarter wavelength restriction, and larger devices may by impractical for industrial applications. Furthermore, the axial spacing between HRs may be used to increase the peak attenuation [54]. To further investigate this effect, various axial spacing distances between multiple HRs are investigated to determine the optimal spacing that maximizes attenuation at the frequency of interest.

Multiple Helmholtz resonators with cavity volumes of either 0.33 L or 1 L were constructed and tuned for the 150 Hz frequency of interest. The use of multiple HRs was first considered in the resonant test pipe in two configurations: (1) multiple HRs placed at the same acoustic pressure antinode (i.e. circumferentially around the pipe), as shown

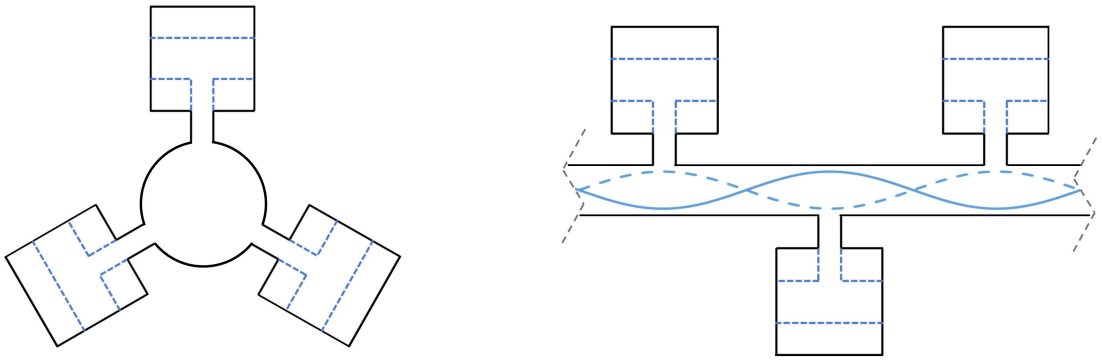

(a) (b)

Figure 4.7: Schematic showing configurations of multiple HRs tested relative to standing wave: (a) Multiple HRs at same acoustic pressure antinode, and (b) Multiple HRs at different acoustic pressure antinodes.

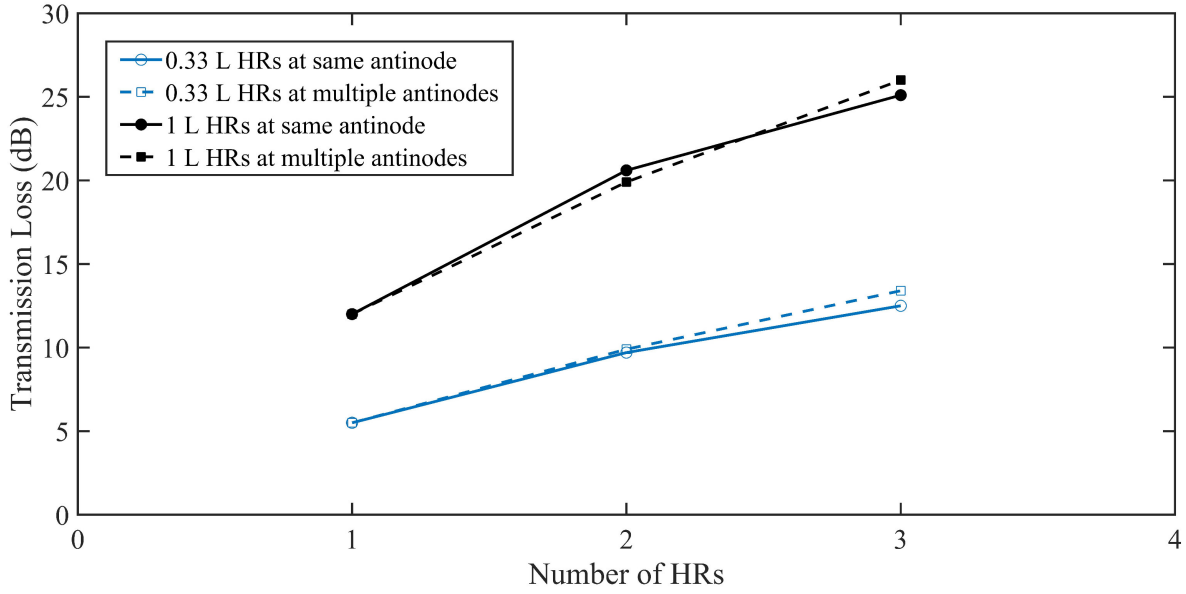

Figure 4.8: Transmission loss values at 150 Hz for multiple 0.33 L or 1 L HRs at the same or different acoustic pressure antinodes.

in Figure 4.7(a) and (2) multiple HRs placed along different acoustic pressure antinodes, as shown in Figure 4.7(b). For each of these configurations, multiple HRs with identical geometries were inserted at the locations shown and their transmission loss was evaluated. The TL magnitude at 150 Hz was extracted for comparison, and the results are shown in Figure 4.8. The results show a nearly linear increase in TL with an increase in the number of HRs, whether they are inserted at the same or multple acoustic pressure antinodes. This shows that multiple HRs tuned for the same frequency can be used to increase the peak attenuation. It also shows there is flexibility regarding the use of multiple HRs; they can be inserted at multiple axial locations along a pipeline or circumferentially around the pipe at a single axial location.

It is also interesting to observe that the TL achieved by three 0.33 L HRs is actually slightly larger than that achieved by a single, 1 L HR. Three 0.33 L HRs yield a TL of approximately 13 dB, while a single 1 L HR yields a TL of about 12 dB. While they are nearly equivalent in terms of total volume, the slight increase in damping achieved using multiple, smaller-volume HRs is attributed to the increase in viscothermal losses at their necks. This is because the total neck lengths of three 0.33 L HRs are much larger than the neck length of a single 1 L HR, which results in larger viscothermal losses as the fluid masses in the necks oscillate during excitation. This finding shows that a single, large-volume HR can be 'split' into multiple smaller HRs with nearly equivalent total volume, provided that the smaller HRs are tuned to target the same frequency of interest. Practically speaking, this means that multiple, relatively smaller devices can be used to increase the magnitudes of damping, especially for low frequencies.

As previously discussed, TL measurements are independent of the test section's resonance. Therefore, the TL for multiple HRs at the same antinode or multiple antinodes corresponds to the TL at the same axial location or with an axial spacing of $\lambda/2$, respectively. In order to methodically investigate the effect of axial spacing between HRs, TL measurements were taken for two 1 L HRs with various axial spacing distances. The

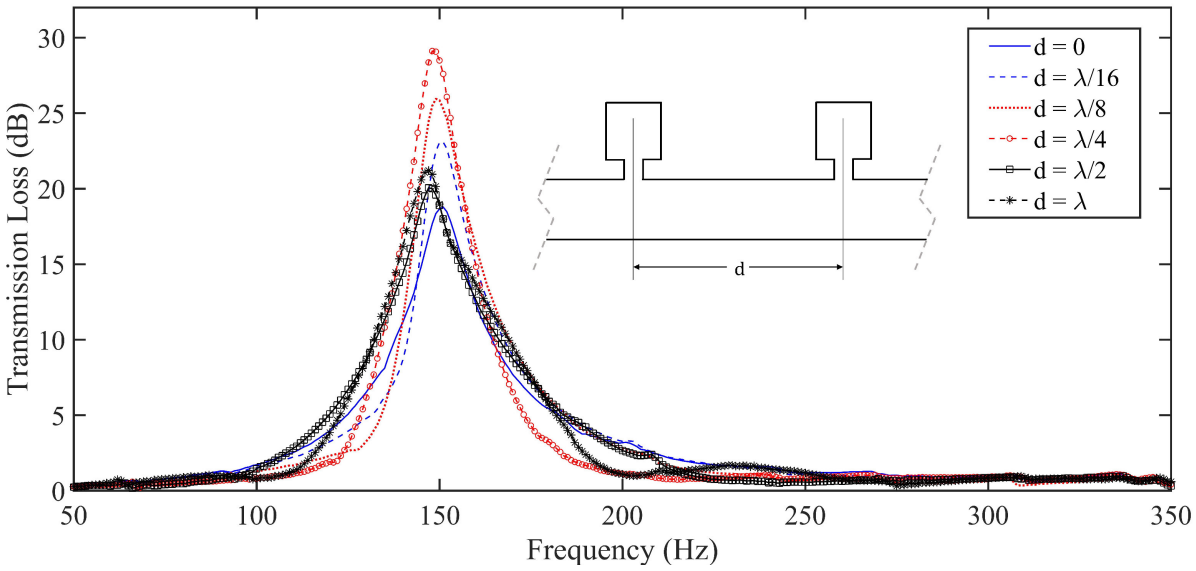

Figure 4.9: Transmission loss for two 1 L HRs with different axial spacing distances.

results are shown in Figure 4.9. It can be seen that the curve is highly dependent upon the axial spacing of the HRs, with both the peak and quality factor of the curve changing with the spacing. In particular, it is interesting to note the significant increase in TL with a spacing of $\lambda/8$ or $\lambda/4$. The peak TL goes from approximately 19 dB when $d = 0$ to nearly 29 dB for $d = \lambda/4$, and then decreases to around 20 dB for $d = \lambda/2$ or $d = \lambda$. It should also be noted that the curves with relatively lower peak TLs (ex. $d = 0$) have broader peaks, while those with higher TL peaks (ex. $d = \lambda/4$) have sharper peaks. The axial spacing distance therefore determines both the peak amplitude and bandwidth of transmission loss.

To verify that the effect of axial spacing observed is not a product of the experimental setup, two additional HRs were constructed with resonant frequencies of 210 Hz. The TL curve for the 210 Hz HR is shown in Figure 4.10. The peak magnitude is around 15 dB at 210 Hz. Two of these HRs were inserted into the pipeline with various spacings relative to the wavelength of 210 Hz, and the transmission loss was measured. The results are shown in Figure 4.11, which show similar trends to those seen for the 150 Hz resonators.

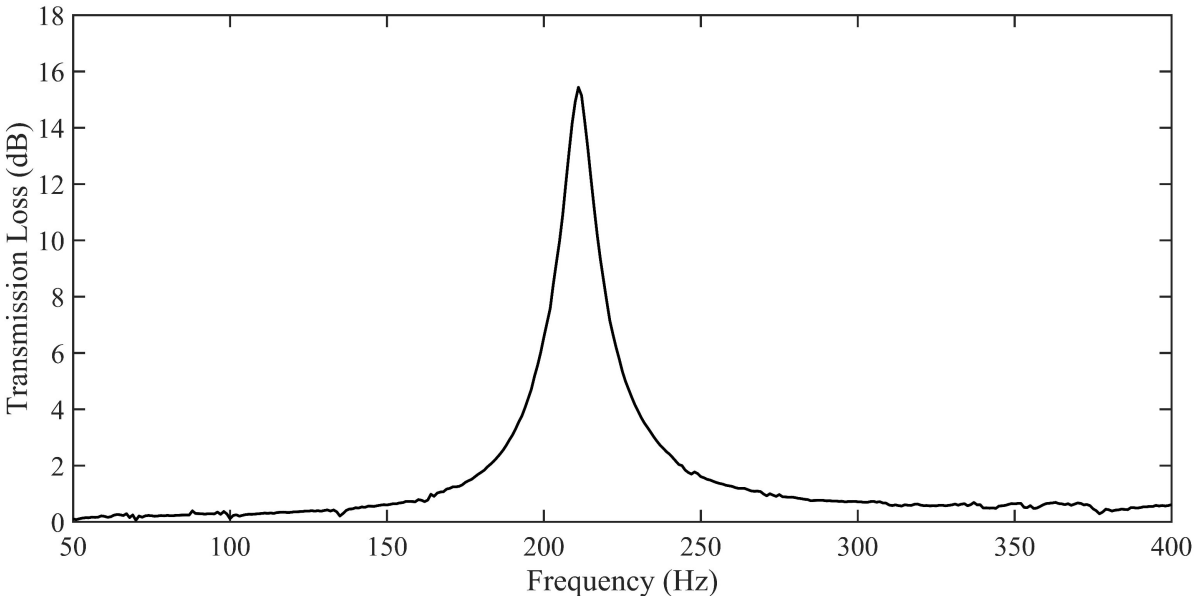

Figure 4.10: Transmission loss of HR tuned with resonant frequency of 210 Hz.

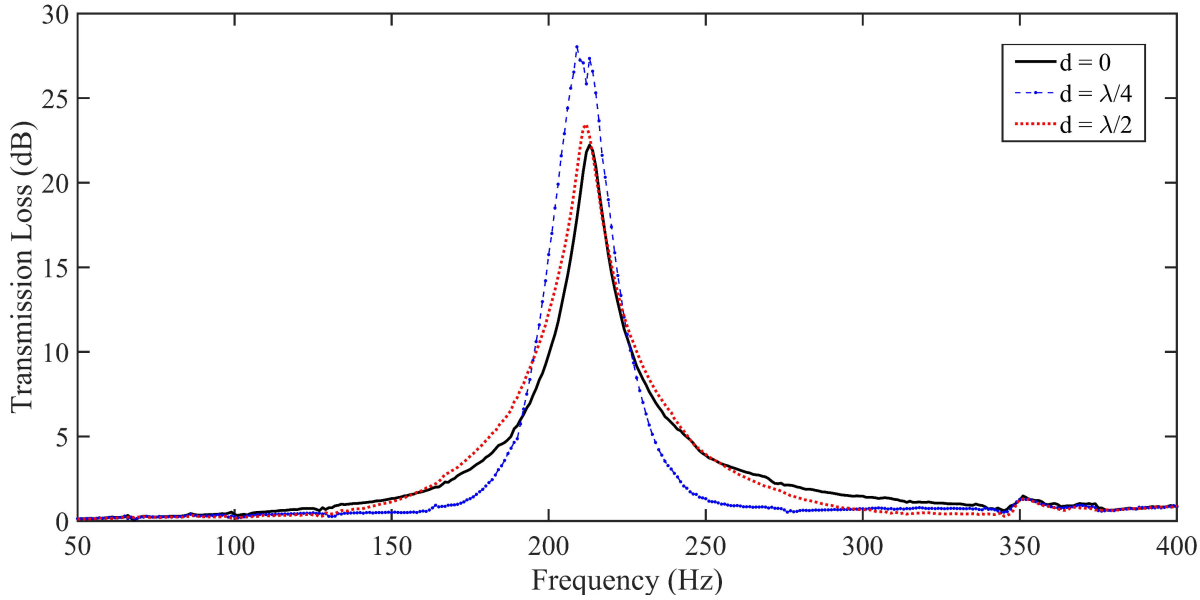

Figure 4.11: Transmission loss for two 210 Hz HRs with different axial spacing distances.

A spacing of $\lambda/4$ yields a peak TL of 28 dB, which corresponds to an increase compared with a spacing of zero (TL = 22 dB) or $\lambda/2$ (TL = 23 dB). This verifies that the spacing between the HRs, referenced using the wavelength of their resonant frequency, can be adjusted to affect both the peak magnitude and bandwidth of attenuation. This suggests that there is some form of coupling between the two HRs with a spacing of $\lambda/4$ that results in an increased energy absorption at their resonant frequency, which is examined in the following chapter.

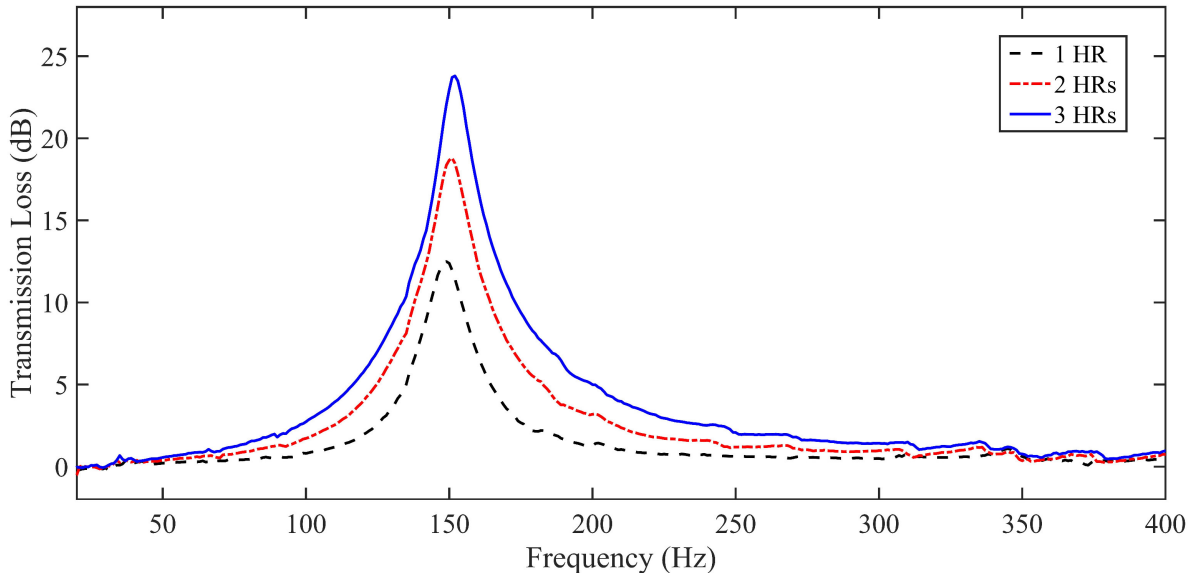

Figure 4.12: Transmission loss of one, two, or three 1 L HRs inserted at the same axial location.

The effect of axial spacing on the TL of multiple HRs can be considered in terms of energy storage, or noise attenuation, capacity, as discussed by Cai and Mak [54]. The area under the TL curve, i.e. energy storage capacity, quantifies the amount of energy stored by the damping device(s). The effect of increasing the number of HRs on the noise attenuation capacity can easily be seen by considering the TL of one, two, or three 1 L HRs inserted at a single axial location, as shown in Figure 4.12. The area under the curve increases with the number of HRs, as shown in Table 4.1. Furthermore, the effect of

Table 4.1: Area under TL curve for 1, 2, or 3 1 L HRs.

	Area under TL curve		
	Spacing		
Number of HRs	$d = 0$	$d = \lambda/4$	$d = \lambda/2$
1	510.2	-	-
2	956.5	956.9	959.9
3	1318	1222	1382

periodic spacing on the energy storage capacity can be considered for multiple HRs. The periodic spacing between devices should affect the frequency, bandwidth, and amplitude of attenuation, but not the energy storage capacity. When the noise attenuation capacity is considered in the present experimental study, it is observed that the areas under the TL curves for the various axial spacing distances is very similar, as shown in Table 4.2. This finding corroborates the theory for energy storage capacity, as it shows that the area under the TL curve is nearly unaffected by the axial spacing between HRs. In summary, it can be seen that an increase in the number of HRs will increase both the peak and the bandwidth of the TL, resulting in an increase in energy storage capacity. However, the periodic spacing between a given number of HRs will have a minimal effect on the energy storage capacity, and only affect the shape of the TL curve.

It is also of interest to consider the insertion loss achieved by multiple HRs, since the magnitudes of damping are heavily dependent upon the device location, as discussed in the previous section. To investigate this, multiple 1 L HRs were inserted into the off-resonant test pipe. The results for the IL of two or three 1 L HRs inserted into the pipeline with various axial spacing distances is shown in Figure 4.13. It is observed that multiple HRs at the same axial location (i.e. $d = 0$) yield similar IL values to those with relatively larger spacing distances, such as $d = \lambda/2$ or $d = \lambda$. For two HRs, the IL is around 15 dB, while for three it is approximately 20 dB for these spacing distances. The

Table 4.2: Area under TL curves for two 1 L HRs with various axial spacing distances (see Figure 4.9).

Spacing	Peak TL (dB)	Area under TL curve
$d = 0$	18.8	956.5
$d = \lambda/16$	23.1	955.7
$d = \lambda/8$	26.0	929.1
$d = \lambda/4$	29.1	956.9
$d = \lambda/2$	20.1	959.9
$d = \lambda$	21.2	935.0

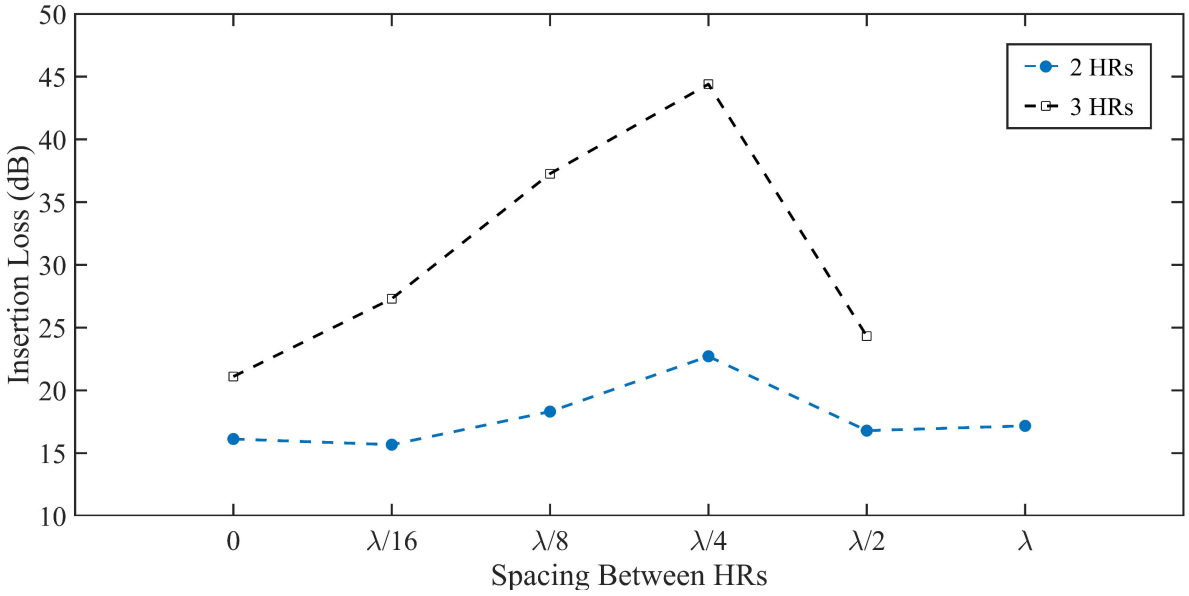

Figure 4.13: Insertion loss of two or three 1 L HRs inserted into the pipeline with various axial spacing distances.

attenuation increases for a spacing of $\lambda/8$, and is maximal at a spacing of $\lambda/4$, yielding IL values of 23 dB with two HRs and close to 45 dB with three HRs. The IL therefore

follows the same trend as the TL, with the highest damping achieved with a spacing between HRs of $\lambda/4$.

In an acoustically resonant system, multiple HRs can be strategically inserted considering the effects of HR location discussed in the previous section. This is particularly useful in systems where characterizing the acoustic waveforms is impractical. In systems with a discrete acoustic excitation source, such as a pump or compressor with constant operating point, the frequency of excitation is known. The speed of sound, c, is a function of the working fluid, the piping material and geometry, and temperature. The wavelength of acoustic excitation can then be found using $\lambda = c/f$. Therefore, although the precise waveform in the pipeline will not be known, multiple HRs can be inserted into the pipeline with axial spacing distances associated with the wavelength, ensuring that some HRs will be close to an acoustic pressure antinode, a location that is known to yield high acoustic attenuation.

For example, three evenly spaced HRs inserted along a quarter wavelength will ensure that at least one one HR is close to an acoustic pressure antinode. To investigate the effectiveness of this configuration, multiple HRs were added at locations 'A', 'M', and 'N' of the resonant pipe test section, as shown in Figure 4.14(a). The IL measurements for three HRs at these locations were compared to those for three HRs either at the same or different acoustic pressure antinodes, as shown in Figures 4.7(a) and (b), respectively. The results are shown in Figure 4.14(b). It is observed that three HRs placed at the same or multiple antinodes yield a similar insertion loss, with IL values of approximately 19 dB for the 0.33 L HRs and 31 dB for the 1 L HRs. Interestingly, the effects of three HRs placed along a quarter wavelength are different for the 0.33 L and 1 L HRs. For the 0.33 L HRs, the IL is nearly 21 dB, which is a slight increase from the other two arrangements. However, this is achieved without placing all three HRs at acoustic pressure antinodes. It is therefore a useful arrangement, as damping levels similar to those achieved at the optimal locations (i.e. acoustic pressure antinodes) are achieved

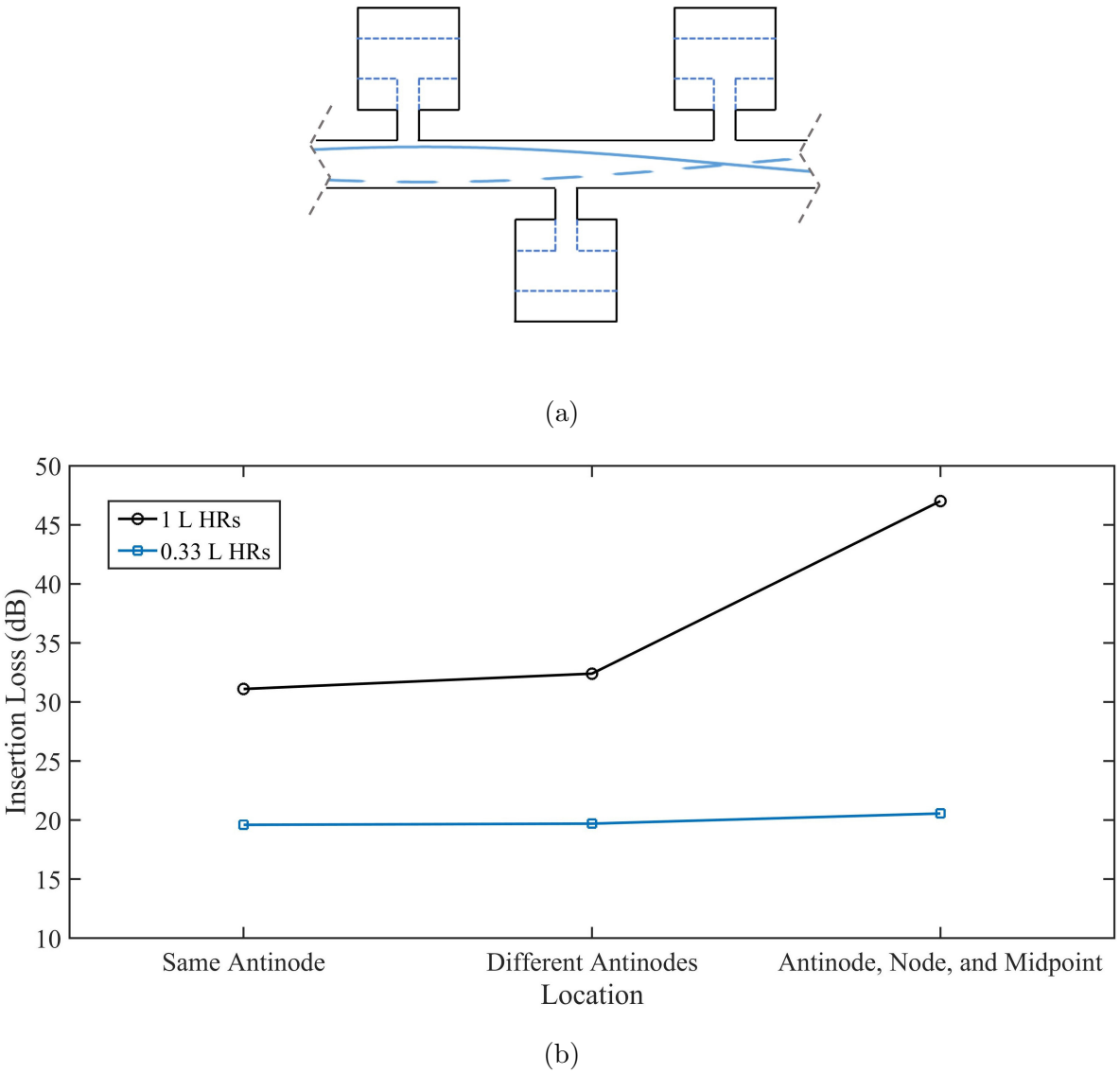

Figure 4.14: (a) Schematic showing three HRs placed along a quarter wavelength, and (b) Transmission loss of three HRs at the same antinode, different antinodes, or along a quarter wavelength.

without having to methodically place all devices at an antinode. Three 1 L HRs along a quarter wavelength yield an insertion loss of 47 dB, which is considerably larger than the attenuation of three 1 L HRs placed at acoustic pressure antinodes. This corroborates the results for multiple HRs with various axial spacing distances discussed above, where it was found that spacing distances of $\lambda/8$ or $\lambda/4$ maximize the peak damping.

4.4 Effect of Mean Flow

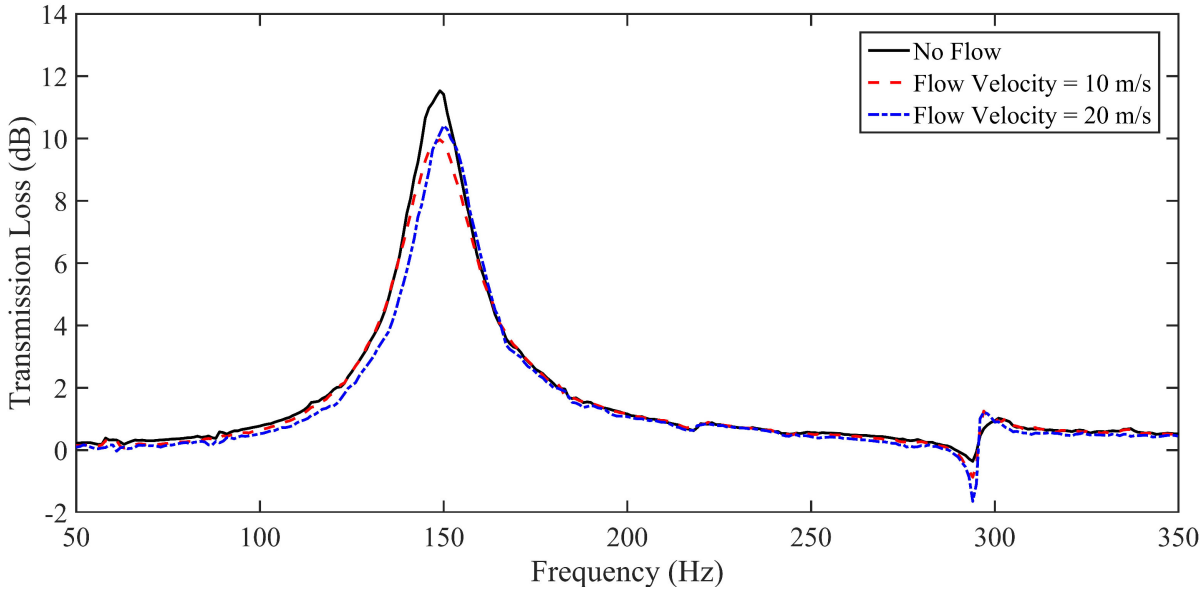

Figure 4.15: Transmission loss of a 1 L HR with various mean flow velocities.

Since mean flows are present in industrial pipeline systems, it is necessary to understand the effects of mean flows on the acoustic performance of any potential damping device. The effects of both mean flow velocity and directionality on the attenuation achieved by HRs was investigated. First, the transmission loss for different mean flow velocities was considered for 'downstream' flows, which are where the mean flow is in the same direction as acoustic wave propagation. The results are shown in Figure 4.15. The results show that both the TL peak frequency and amplitude are slightly affected by the

presence of mean flow. The TL peak, which represents the HR resonant frequency, shifts to slightly higher frequencies with the presence of mean flow. The magnitude of TL is slightly reduced by the presence of mean flow, reducing from around 12 dB for the no flow case to nearly 10 dB with flow velocities of 10 m/s or 20 m/s.

In order to evaluate the effects of both downstream and upstream propagating waves, insertion loss measurements were performed with the HR at different axial locations of the resonant test pipe. Downstream flow measurements were taken with the excitation source near the inlet, and the results are shown in Figure 4.16. It can be seen that the magnitudes of attenuation decrease slightly with an increase in downstream mean flow velocity. Upstream flow measurements, where the incident acoustic waves propagate in the opposite direction to mean flow, were taken with the excitation source near the muffler. The results are shown in Figure 4.17. In this case, it is observed that the magnitudes of insertion loss increase slightly. In other words, the acoustic attenuation achieved by an HR is slightly reduced when the mean flow is in the same direction as the incident acoustic waves, while its acoustic performance is slightly enhanced when the mean flow opposes acoustic wave propagation.

The presence of mean flow on a duct or pipeline system is known to affect both the wavenumber, k, and the viscothermal losses within the system [65]. Both parameters are functions of the mean flow velocity and directionality. The wavenumber is affected by mean flow due to convection effects (i.e. the Dopper effect), whereby the mean flow results in a shift in frequencies of acoustic excitation. The viscothermal losses, which quantify the dissipation in acoustic pressure, are dependent upon the interaction between the acoustic boundary layer and the mean flow boundary layer. These were both considered for the effects of mean flow velocity and directionality on the insertion loss of the HR. However, insertion loss measurements are taken by finding the reduction in sound pressure level caused by inserting a device into a system with a particular flow velocity and direction. The effects of convection velocity and viscothermal losses can

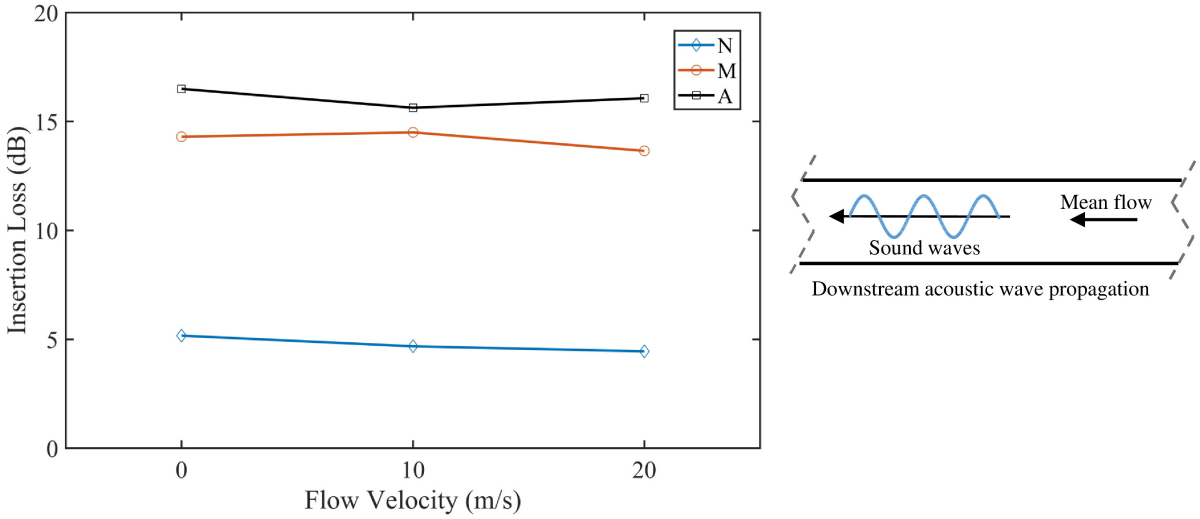

Figure 4.16: Insertion loss of a 1 L HR at various locations with different downstream flow velocities.

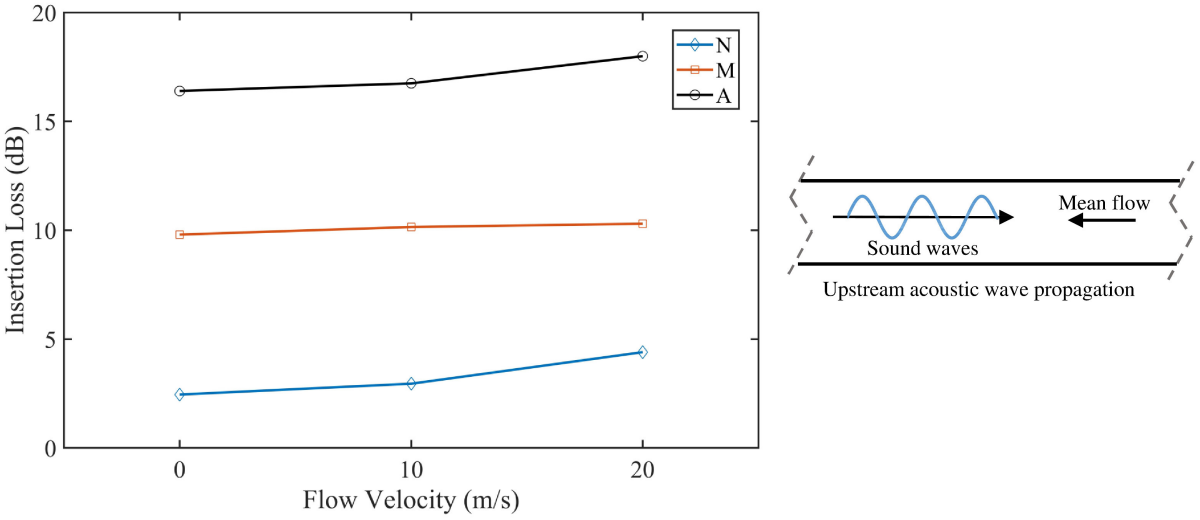

Figure 4.17: Insertion loss of a 1 L HR at various locations with different upstream flow velocities.

therefore not explain the difference between downstream and upstream flows, since these effects should be the same before and after a damping device is inserted into a system. The effect of flow directionality may be explained by the direction of flow separation and impingement across the opening of the HR neck relative to the mean flow, which may be sensitive to flow directionality.

Chapter 5

Mechanism of Attenuation

The trends discussed in the previous chapter show the effects of various HR configurations and sizes in both resonant and off-resonant test pipes. While these trends are important for any practical considerations, i.e. the implementation of HRs in duct or pipeline systems, it is also of interest to shed light on the underlying reasons for the behaviour seen. This chapter focuses on acoustic pressure measurements taken within the test pipe, as well as within the HR cavity volume(s), to help clarify the mechanism of attenuation of Helmholtz resonators in pipeline systems.

5.1 Pressure and Phase Measurements in a Single HR

First, a single HR attached to the pipeline system was considered. In this case, a 1 L HR was attached to the off-resonant test pipe. Acoustic pressure measurements were taken inside the HR cavity volume and inside the pipeline at the axial location where the HR was attached, as shown in Figure 5.1(a). The ratio of acoustic pressure between the HR and the pipeline was compared to show the amplification of pressure in the HR relative to the pipeline. The phase difference between the two measurements was also measured.

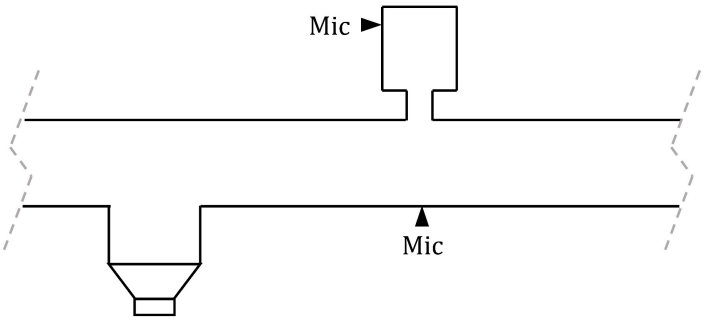

(a)

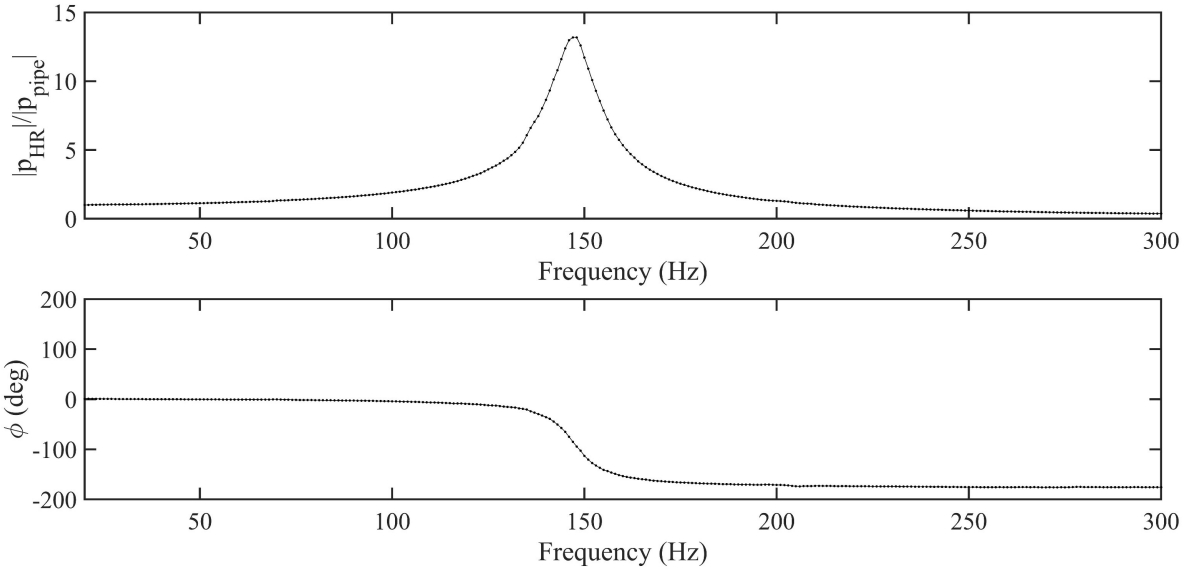

(b)

Figure 5.1: (a) Schematic of acoustic pressure measurements in HR cavity volume and in the pipeline at the HR junction, and (b) Pressure ratio and phase difference measurements between the HR cavity volume and pipeline at the HR junction for a 1 L HR.

The results are shown in Figure 5.1(b). The pressure ratio measurements clearly show an amplification in the HR cavity volume pressure relative to the pipeline, with the peak centered close to the HR resonant frequency of 150 Hz. This is indicative of a transfer of energy from the main pipeline to the HR sidebranch.

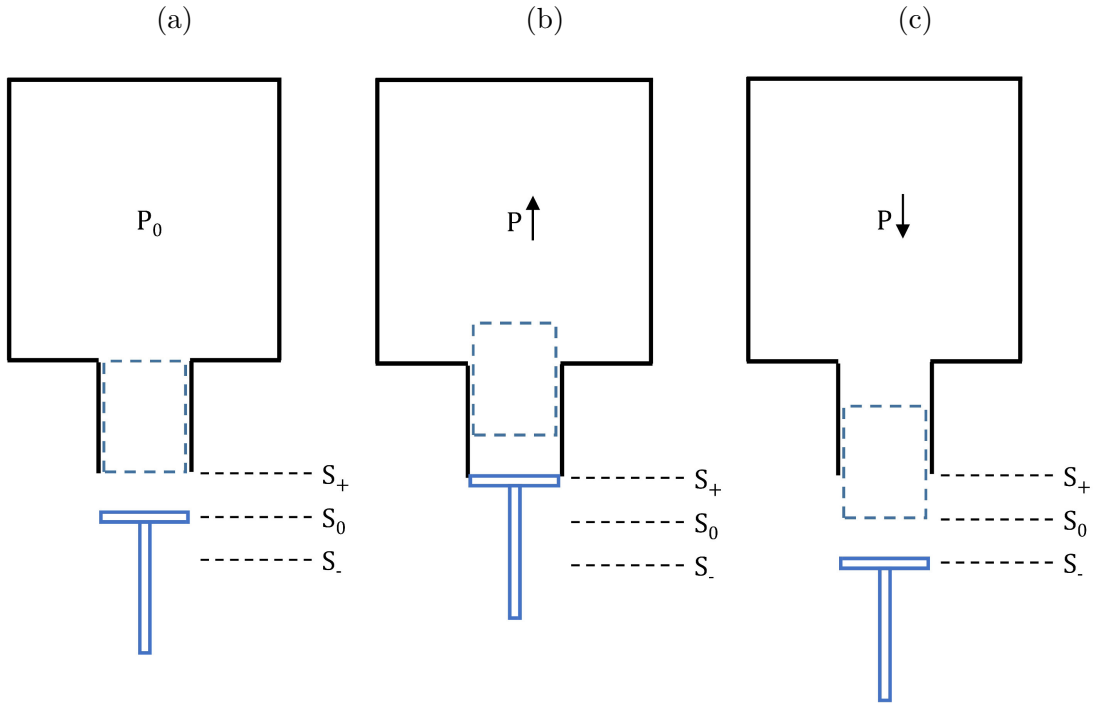

Figure 5.2: Schematic of source excitation at HR neck opening in different positions: (a) Equilibrium position, S_0, (b) maximum position, S_+, and (c) minimum position, S_-.

Furthermore, the phase measurements between the HR cavity and the pipeline, as shown in Figure 5.1, reveal a phase difference of nearly 90 degrees at the 150 Hz frequency. The importance of this phase difference can be understood by considering the schematic shown in Figure 5.2. A periodic source acting over the neck opening of the HR is represented using a piston, which oscillates through equilibrium position S_0 to its maximum at S_+ and minimum at S_-. The HR is treated using the lumped parameter model previously discussed, whereby the mass of fluid in the neck (represented as the dashed box) oscillates as the pressure in the cavity volume compresses and rarefies. At

the source equilibrium position S_0, the pressure in the cavity volume is also at its equilibrium position, i.e. zero acoustic pressure. When the source reaches its maximum position of S_+, the mass of fluid in the neck is pushed to its maximum displacement into the cavity volume, and the acoustic pressure in the cavity volume is accordingly at its maximum. Conversely, when the source is at its minimum position S_-, the mass of fluid in the neck is pulled to its furthest position outwards from the cavity, and consequently the pressure in the cavity volume is also at its minimum. In other words, the source at the neck opening moves in phase with the acoustic pressure in the cavity volume. Therefore, the phase difference between the HR cavity and the pipeline is the same as the phase difference between the neck opening and the pipeline. This is significant considering the literature regarding other sidebranch damping devices, such as the Herschel-Quincke tube [35] or quarter wave resonator [30]. For these devices, a phase difference of 90 degrees shows that the sidebranch junction is a location of minimum acoustic pressure, a condition that is necessary to sustain the resonance within the sidebranch. The phase difference of 90 degrees at 150 Hz, as shown in Figure 5.1, thus confirms that the HR acts as a minimum acoustic pressure at its junction with the pipeline.

The imposition of a minimum acoustic boundary condition at the HR's junction with the pipeline can be used to explain the effectiveness of HRs at various locations in resonant and off-resonant pipelines. From the results discussed in the previous section, it was seen that the insertion loss in a resonant system was highly dependent on location, with maximal attenuation at the acoustic pressure antinode and minimal attenuation at the node. This can be understood from the perspective of the mechanism of attenuation discussed here. When the HR is placed at the acoustic pressure antinode, it imposes a minimum acoustic pressure, thereby disrupting the coupling that results in acoustic resonance. Accordingly, the HR achieves maximal damping at this location. Conversely, when the HR is placed at a node, it imposes a minimum acoustic pressure at an existing minimum pressure location. The HR does not effectively disrupt the coupling that results

in acoustic resonance, and the acoustic damping is minimal.

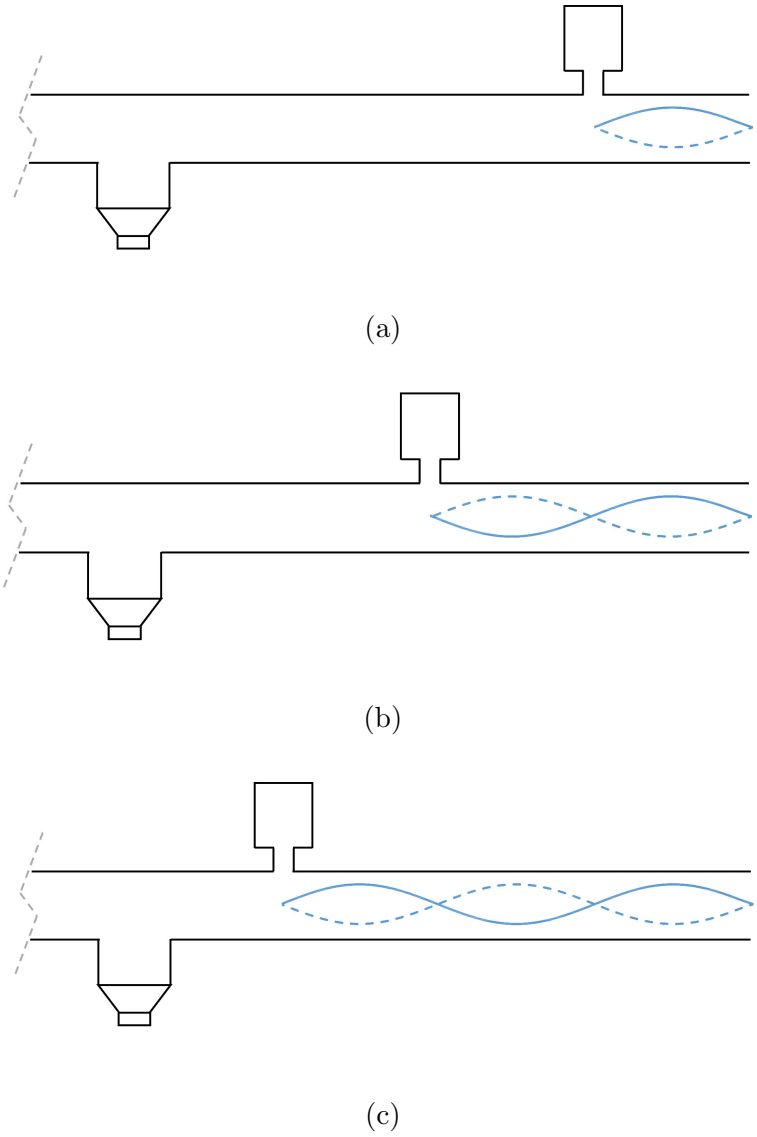

Figure 5.3: Schematic of constructive inteference between HR and open end for: (a) $d = \lambda/2$, (b) $d = \lambda$, and (c) $d = 3\lambda/2$.

The attenuation achieved in an off-resonant pipeline was seen to be relatively constant, with the exception of when the HR was inserted at distances of λ or $3\lambda/2$ from the open end. This is caused by an interaction between the HR junction and the open end condition that results in constructive interference. Since both locations act as acoustic pressure

minima, distances between the two that correspond to multiples of $\lambda/2$ will result in a coupling, i.e. an amplification of acoustic pressure. This is illustrated schematically in Figure 5.3, which shows the shortest three distances between the HR and open end that result in a coupling, i.e. (a) $\lambda/2$, (b) λ, and (c) $3\lambda/2$. Accordingly, these locations will yield decreased levels of acoustic damping. Therefore, the HR locations that result in a coupling between the end terminations and the HR junction should be avoided if possible. In particular, relatively shorter distances between the end termination and the HR should be avoided because the coupling will be stronger for shorter distances than for larger ones. For example, the IL at a distance of $d = \lambda/2$ or $d = \lambda$ will be even lower than the IL for higher multiples of $\lambda/2$, such as $d = 3\lambda/2$ or $d = 2\lambda$. In other words, although the distances that result in a coupling between an HR and end termination should be avoided altogether to maximize acoustic damping, the strength of the coupling can be minimized by increasing the distance between the HR and end termination.

5.2 Pressure, Phase, and Reflection Coefficient Measurements for Two HRs

Another important finding from the previous chapter was the attenuation of multiple HRs with various axial spacing distances. It was found that an axial spacing of $\lambda/4$ was optimal for increasing peak attenuation. For acoustic waves propagating through a pipeline, the incident acoustic pressure will either be transmitted, reflected, or absorbed. Therefore, reflection coefficient measurements can be used to quantify the ratio of reflected to incident acoustic pressures in the main pipeline at the HR junctions. For the reflection coefficient measurements presented, two 1 L HRs with different axial spacing distances were inserted into the test pipe. As shown in Figure 5.4(a), the reflection coefficient upstream of both HRs, R1, and of the downstream HR, R2, was measured. The results are shown in Figure 5.4(b). It can be seen that the reflection coefficient upstream

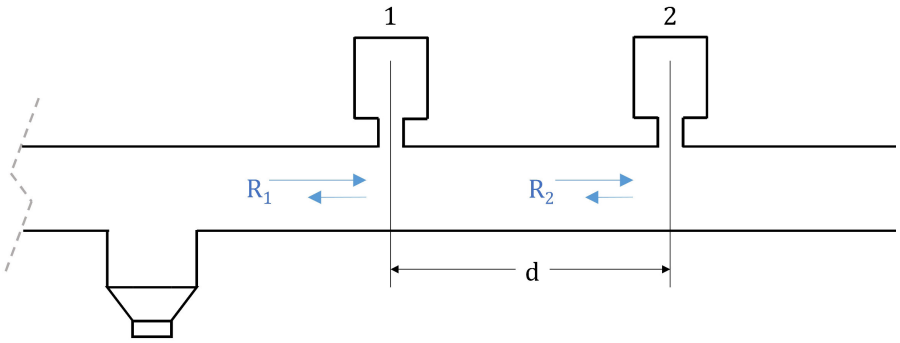

(a)

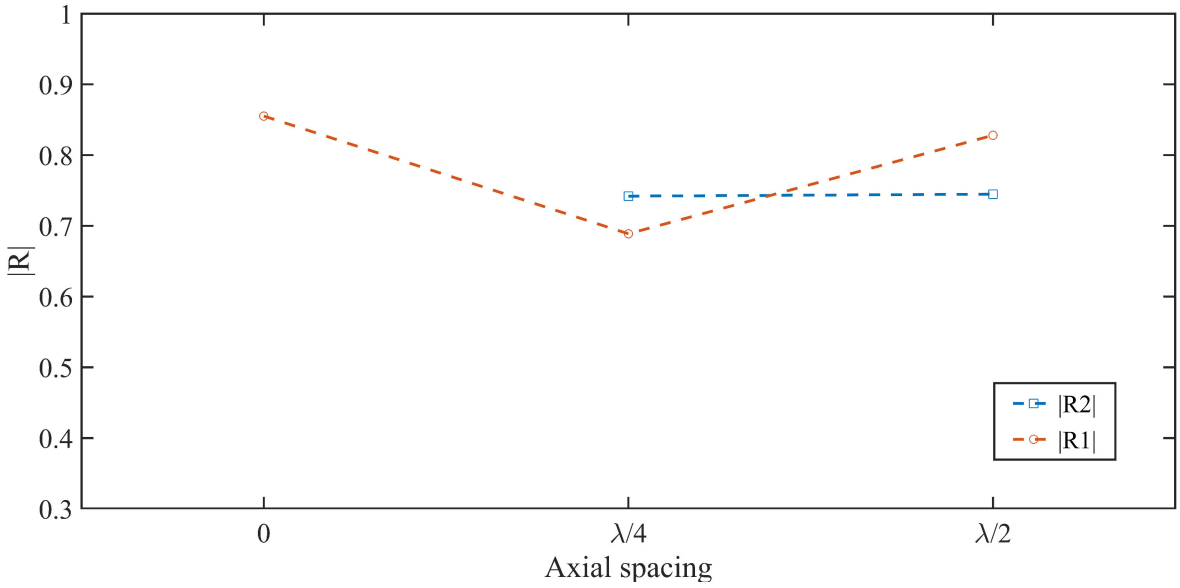

(b)

Figure 5.4: (a) Schematic of reflection coefficient measurements for two HRs, and (b) Reflection coefficient extracted at 150 Hz for multiple HRs with different axial spacing distances.

of both HRs is similar for a spacing of zero or $\lambda/2$, but decreases with a spacing of $\lambda/4$. Therefore, at a spacing of $\lambda/4$, a larger portion of the incident wave must be transmitted or absorbed. However, from the transmission loss measurements in the previous chapter, it is known that this spacing yields a relatively high peak TL, i.e. the ratio of transmitted to incident acoustic pressure is low. Additionally, the reflection coefficient of the second HR, R2, was very nearly the same value for axial spacing distances of $\lambda/4$ and $\lambda/2$, indicating that the second HR does not behave differently for the two spacing values. This means that at the axial spacing of $\lambda/4$ results in an increased absorption of energy, seemingly within to the HR closest to the source.

In order to quantify the energy transferred to the sidebranch HRs, measurements were taken within the HR cavities for two HRs with different spacing distances as shown in Figure 5.5(a). Location 1 refers to the upstream HR location, closest to the source, while location 2 refers to the HR furthest from the source. The results are shown in Figure 5.5(b), which shows the ratio of the magnitude of acoustic pressures between the 2 HRs, as well as the phase difference between the two measurements. Comparing the ratio of acoustic pressure amplitudes, it can be seen that the value is unity when $d = 0$, i.e. when the HRs are placed at the same axial location. This means that the acoustic pressures in the two HRs are the same, so that an equivalent amount of energy from the pipeline is transferred to each HR. The phase difference is zero for this spacing. This is expected because the excitation in a pipeline is one-dimensional for frequencies below the cutoff, so the excitation at the neck junctions for two HRs located at the same axial location is identical. For $d = \lambda/2$, the pressure ratio is nearly unity and the phase difference is close to 180 degrees at 150 Hz. This shows that, at their resonant frequency, each HR absorbs an equivalent amount of acoustic energy from the pipeline. The spacing of $d = \lambda/4$ shows an interesting ratio of pressure amplitudes between the HRs, with a value of nearly 6 at the resonant frequency of 150 Hz. This means that the pressure amplitude in the HR closest to the source is almost six times greater than that in the HR furthest from

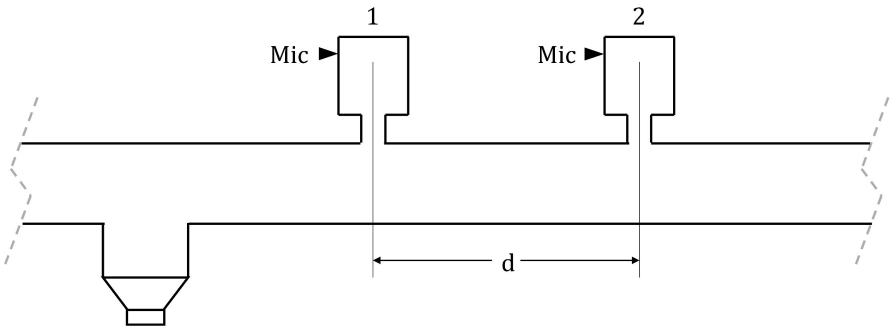

(a)

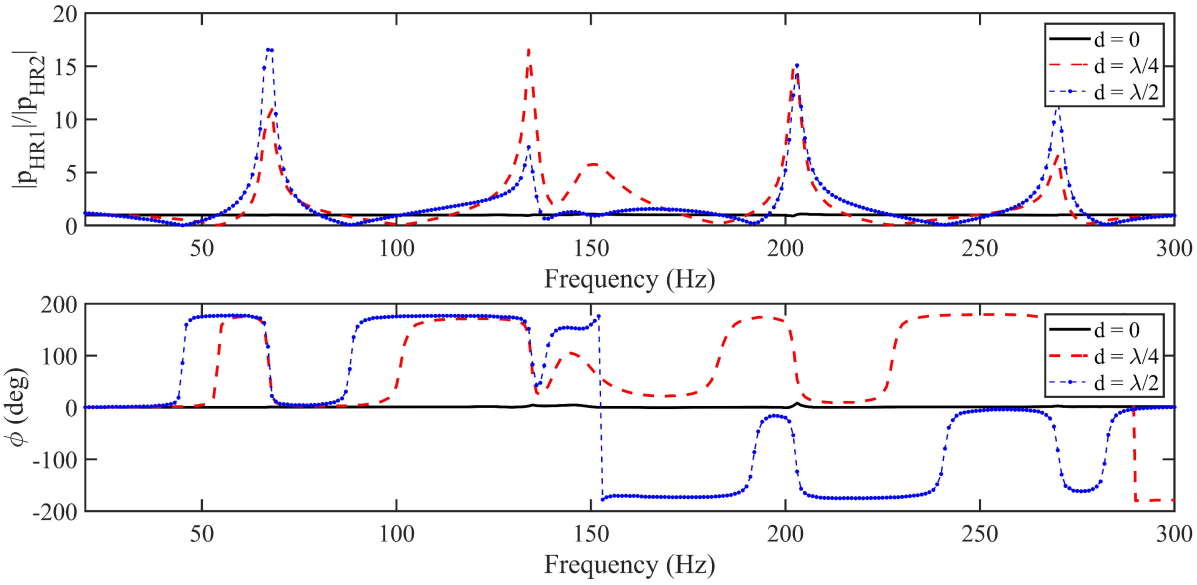

(b)

Figure 5.5: (a) Schematic of acoustic pressure measurements within two HR cavities, and (b) Ratio of acoustic pressures and phase difference between two HR cavities with different axial spacing distances.

the source. This suggests that there is a coupling between the HRs at a spacing of $\lambda/4$ that results in more energy from the pipeline being transferred to the upstream HR than the downstream HR. Additional peaks can be noted in the pressure ratio spectra at 68 Hz, 134 Hz, 203 Hz, and 270 Hz. These are caused by acoustic resonance in the test section. However, while these frequency components are present in the HRs, they do not coincide with the natural frequency of the HRs and therefore do not affect the frequency or strength of resonance in the HRs.

Chapter 6

Effect of Pressure Amplitude

Another important consideration regarding the applicability of Helmholtz resonators is their sensitivity to incident pressure amplitudes. Several authors have noted that increasing the amplitudes of the incident acoustic pressure results in an increase in the acoustic resistance of the neck, i.e. an increase in the energy losses within the HR [36, 66, 67]. As previously discussed, the fluid in the neck of the resonator oscillates during excitation at its resonant frequency. If the pressure amplitudes are sufficiently high, jets are formed as the flow passes through the neck orifice, as shown schematically in Figure 6.1. It should be noted that this 'jet-flow' occurs during both the (a) 'in-flow' and (b) 'out-flow' parts of the cycle, which correspond to the motion of the neck fluid into and away from the cavity volume, respectively. The interaction between the formed jets and the surrounding fluid results in vortices that dissipate into turbulence [39]. The associated energy losses caused by jet flow comprises one of two major sources of damping within the resonator - the other being the frictional, or viscothermal, losses that occur along the walls of the neck. This damping depends on the acoustic excitation frequency and amplitude, as well as the orifice geometry. Necks with low length-to-radius ratios (l_n/r_n) are more sensitive to the jet-flow effect, as shown by Hersh et al. [68].

The effects of high-amplitude excitation and the jet losses arising therefrom have been

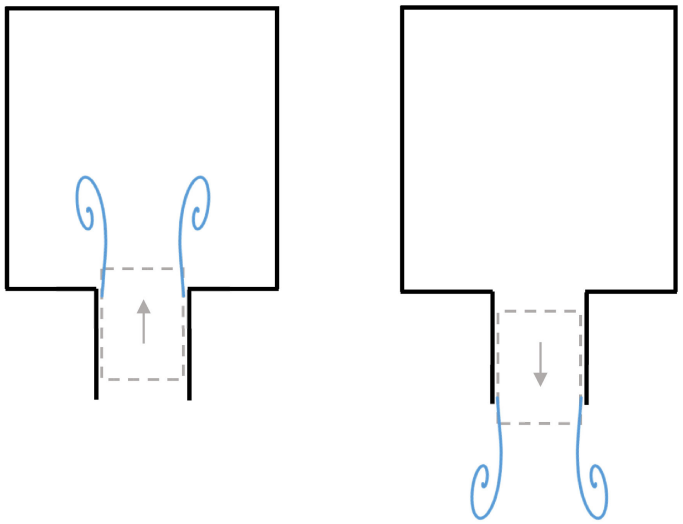

Figure 6.1: Schematic of jet-like flow through an HR neck during (a) 'In-flow': as the fluid in the neck enters into the cavity volume, and (b) 'Out-flow': as the fluid in the neck exits away from the cavity volume.

considered insofar as they result in an increase in the resistance of an HR; their effects on the transmission loss achieved by an HR has not been explicitly investigated. Therefore, experiments were conducted to study the effects of incident pressure amplitude on the acoustic damping achieved by an HR. To control the acoustic pressure provided into the pipeline, the power level input into the source (P_s) was adjusted using an amplifier. The transmission loss was then evaluated with various source power levels.

First, the transmission loss of an expansion chamber (EC) and quarter wave resonator (QWR) were considered for various source excitation levels. The results are shown in Figure 6.2, which shows the TL spectra for both devices for various input power levels. For both devices, it can be seen that the transmission loss spectra is unaffected by changes in power level. This corroborates one of the most commonly cited attributes of transmission loss as a measurement technique - that it is independent of the source [58, 69]. Since TL is not a property of the source characteristics or end terminations, it

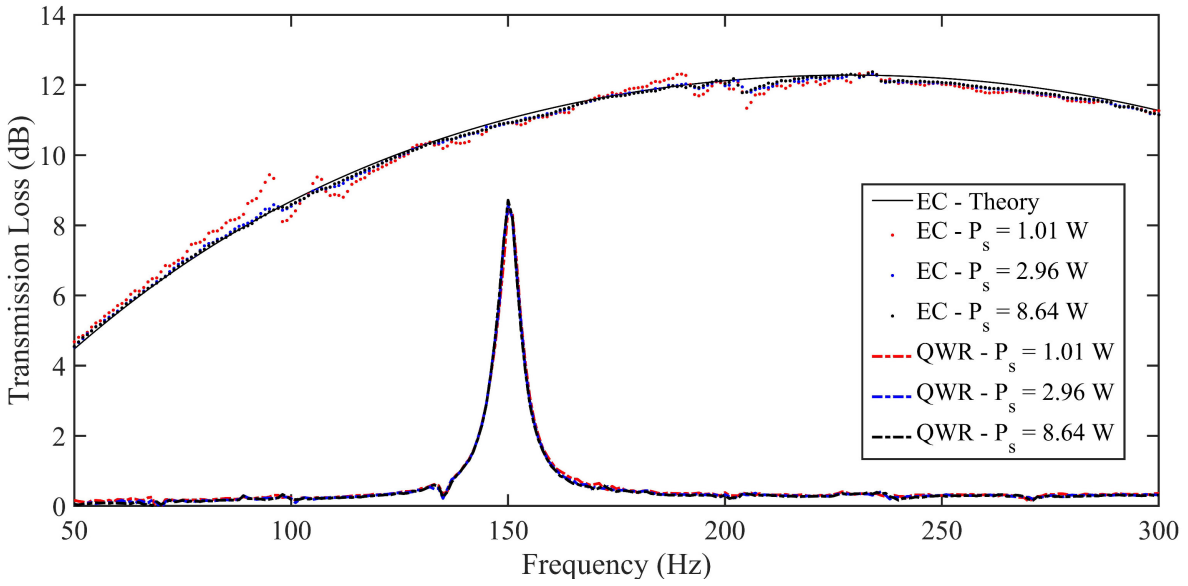

Figure 6.2: Transmission loss of an expansion chamber (EC) (d = 11", l = 15") and quarter wave resonator (QWR) (d = 1", l = 22") for various input power levels.

is often referred to as a property of the 'muffler proper', i.e. the damping device itself [56].

However, while the TL of the expansion chamber and quarter wave resonator are unaffected by pressure amplitude, Figure 6.3 shows that the TL of the 1 L HR is, in fact, sensitive to the source excitation level. In particular, attention should be paid to the decrease in peak attenuation with the increase in source power, even though the peak frequency remains unchanged. An input power of 1.01 W yields a peak TL of over 14 dB, compared with 12 dB for an input power of 8.64 W. Only the response in and around the resonant frequency is changed, showing a higher quality factor of the transmission loss peak for lower source power levels. This is attributed to the increased damping within the HR from increased jet losses at the HR neck at high incident pressure amplitudes. The pressure amplitude can therefore have a considerable effect on the acoustic damping achieved by an HR.

In order to investigate the sensitivity of various HR geometries to the effects of incident

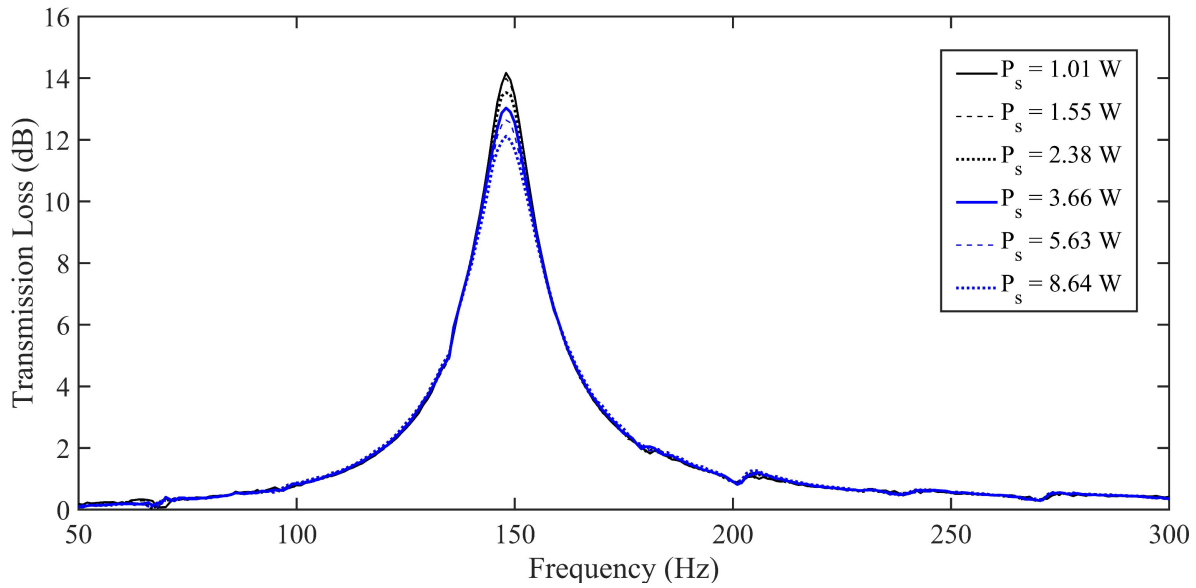

Figure 6.3: Transmission loss of a 1 L HR (l_{neck} = 1.5") for various input power levels.

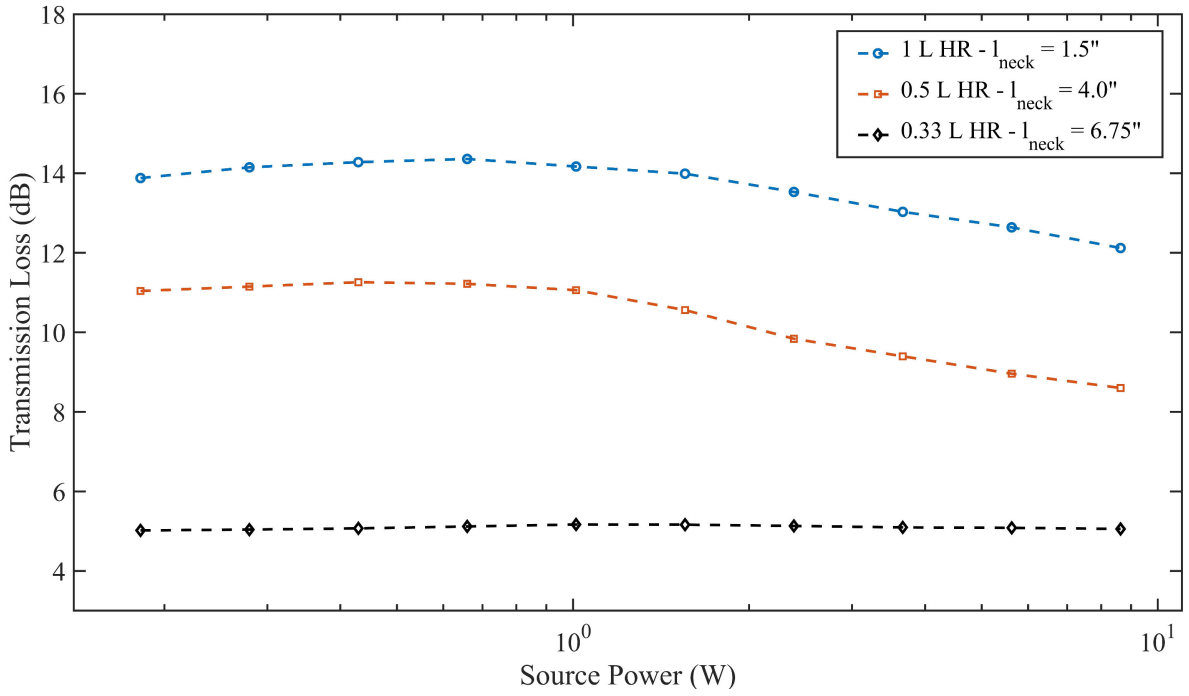

Figure 6.4: Peak TL values (extracted at 150 Hz) of a 0.33 L HR (l_{neck} = 6.75"), 0.5 L HR (l_{neck} = 4.0"), and 1 L HR (l_{neck} = 1.5") for various input power levels.

acoustic pressure amplitude, TL measurements for the 0.33 L and 0.5 L HR were also taken with various input power levels. A comparison of the peak TL values at 150 Hz for all three HR sizes is presented in Figure 6.4. It can be seen that the transmission loss of both the 0.5 L and 1 L HRs are sensitive to the incident pressure amplitude. For low excitation levels, the TL is relatively constant, and as the source excitation is increased further, an appreciable decrease in transmission loss is observed. The TL of both the 0.5 L and 1 L HRs decreases by nearly 2 dB over the tested range of power levels. However, the TL of the 0.33 L HR is unaffected by pressure amplitude, maintaining a TL of nearly 5 dB for all input power levels. This is caused by its longer neck length, which makes it less prone to the jet-flow effect and the associated losses. This trend is also indicative of a threshold HR neck length at which the TL is not sensitive to the incident pressure amplitudes, which, although is interesting, is left to further investigation. The important point here is that the transmission loss is dependent upon the magnitude of excitation provided by the source for HRs with small to intermediate neck lengths, which has implications for the use of transmission loss as a measurement technique and for the scaling of HR performace from test apparatuses to industrial systems.

Although transmission loss is often considered to be independent of the source, it has been shown here that the TL of HRs with certain neck lengths is dependent upon the amplitude of source excitation. The peak TL can significantly decrease with increases in the levels of acoustic excitation in the pipeline. Accordingly, care must be taken when TL is used to evaluate the acoustic performace of Helmholtz resonators, particularly for those with short neck lengths. This is especially true if TL is used as a method for benchmarking a device that will be used in an industrial application. It is therefore recommended to evaluate the HR performance at excitation levels similar to those present in the system of intended application, if possible. Otherwise, the TL of an HR can be evaluated for various source excitation levels to obtain a plot similar to that of Figure 6.4, so that the peak TL at an excitation level outside of the testable range can be

approximated.

The effect of pressure amplitude on HR performance should be considered in conjunction with the effects of volume, location, multiple devices, and mean flow discussed in Chapter 4. For example, even though larger volume HRs yield higher damping levels than smaller ones, the difference in achieved attenuation between the various volumes depends on the excitation level. Additionally, it was found that three 0.33 L HRs yield similar attenuation levels to a single 1 L HR (Figure 4.8). Since the smaller volume HRs, which have longer necks, are less sensitive to the effects of excitation amplitude, this makes the use of multiple, small-volume devices even more suitable for application in high-amplitude systems.

As such, the discussions of acoustic damping and the mechanism of attenuation of HRs should be viewed in conjunction with considerations of the sensitivity of HRs to pressure amplitude. This is important for scaling the response of an HR from a test setup to the system of application. Furthermore, it should be noted that transmission loss measurements will be pressure amplitude-dependent for any damping device consisting of one or more orifices. This must be stressed, as the 'source independence' of damping devices is, in fact, only a property of the transmission loss technique to the extent that source excitation amplitude does not affect the response of a damping device.

Chapter 7

Conclusions

The acoustic damping and mechanism of attenuation of Helmholtz resonators have been experimentally investigated in this thesis. An open air loop setup with modular test section lengths was used to quantify the acoustic damping and response of various HR sizes and configurations. First, three HRs with various cavity volumes were constructed and tuned to the 150 Hz frequency of interest, and their transmission loss was evaluated in various pipeline diameters. It was found that larger HR volumes yield higher acoustic damping, and that the increase in pipeline diameter results in a decrease in damping. Next, the effect of HR axial location was investigated for both resonant and off-resonant test sections. For the resonant test pipe, it was found that the insertion loss follows the acoustic pressure distribution of the standing wave, with maximal damping achieved at the antinode and minimal damping at the node. The IL was relatively consistent for the off-resonant test pipe, with discrete dips in the damping noted when the HR was a multiple of a half wavelength from the end termination of the pipeline. The use of multiple HRs was also studied, which showed that multiple, relatively small-volume HRs can be used to achieve similar damping to a single, large-volume HR with similar total volume. The effects of axial spacing between multiple HRs was also studied, and it was found that an axial spacing distance of $\lambda/4$ can be used to maximize the peak acoustic

attenuation. The effect of mean flow velocity and directionality was investigated, which showed that the acoustic attenuation is somewhat sensitive to low Mach number flows.

To shed light on the trends observed for the acoustic damping, additional measurements were taken to clarify the mechanism(s) of attenuation of HRs connected to pipeline systems. First, pressure amplitude and phase measurements were taken for a single HR within the HR cavity and the pipeline at the HR junction. The transfer function measurements reveal an amplification of the HR resonant frequency in the cavity relative to the pipeline, with a phase shift of nearly 90 degrees. This phase shift was considered in conjunction with the lumped parameter model and an acoustic source analysis to show that the HR imposes a minimum acoustic pressure boundary at its junction with the pipeline. This explains the insertion loss trends of an HR in the resonant and off-resonant test pipelines. The mechanism of multiple HRs was first considered using reflection coefficient measurements, which showed that the axial spacing of $\lambda/4$ did not increase the acoustic reflection back to the source, indicating that this spacing may actually result in increased energy absorption from the pipeline. Measurements within the cavity volumes of two HRs with various spacing distances between them were subsequently performed, showing that for the $\lambda/4$ spacing, the HR closest to the source resonates with higher amplitudes than the HR further from the source. This shows that there is a coupling between the two HRs at this spacing, which manifests in the upstream HR absorbing more energy from the pipeline than the downstream HR.

Experiments were also conducted to show the effects of source excitation level on the acoustic damping of HRs. It was shown that, unlike the expansion chamber or quarter wave resonator, the transmission loss of an HR with small to intermediate neck lengths is dependent upon the input power from the source. This is attributed to the jet-flow phenomena that is present in the HR neck at high pressure amplitudes, resulting in additional damping within the HR and, consequently, a decrease in transmission loss along the pipeline. This shows that the pressure amplitude from the source can significantly af-

fect the acoustic damping achieved by a Helmholtz resonator, which should be considered when designing and testing HRs for real-world applications. Moreover, this behaviour shows that the transmission loss technique is not entirely 'source independent', since increases in the amplitude of excitation are seen to decrease the peak transmission loss. Therefore, a range of input source amplitudes should be tested when using transmission loss for damping devices with geometries that consist of one or more orifices.

The experimental results demonstrate that HRs can be incorporated into pipeline systems where discrete acoustic excitation is problematic. The experiments regarding HR volume, location, multiple HRs, and mean flows have shown important trends regarding the utilization of HRs in pipeline or duct systems. It has been shown that the strategic placement of HRs can achieve significant damping without the need for characterizing the pipeline acoustics. Multiple, relatively small HRs have been shown to yield high attenuation for low frequencies, demonstrating their potential use in systems where spatial limitations preclude the use of most other passive techniques. Additionally, measurements have been taken to help clarify the mechanism of attenuation of HRs in pipeline systems, which helps provide an understanding of the behaviour observed. Further experiments reveal that the peak attenuation of an HR may be dependent on the excitation level from the source, which must be considered when scaling the response of an HR to the system of its intended application. The findings of this thesis may be used as a guideline for the utilization of Helmholtz resonators in piping or duct systems where it is desirable to attenuate discrete acoustic excitation.

Bibliography

[1] Lawrence E Kinsler, Austin R Frey, Alan B Coppens, and James V Sanders. Fundamentals of acoustics. *Fundamentals of Acoustics, 4th Edition, by Lawrence E. Kinsler, Austin R. Frey, Alan B. Coppens, James V. Sanders, pp. 560. ISBN 0-471-84789-5. Wiley-VCH, December 1999.*, page 560, 1999.

[2] E ASTM. 2611-09. *Standard test method for measurement of normal incidence sound transmission of acoustical materials based on the transfer matrix method*, 2009.

[3] A Mohany and M Hassan. Modelling of fuel bundle vibration and the associated fretting wear in a candu fuel channel. *Nuclear Engineering and Design*, 264:214–222, 2013.

[4] Brian C Howes, SD Greenfield, and CK Schuh. Acoustic pulsations in reciprocating machinery. *Canadian Acoustics*, 19(4):15–16, 1991.

[5] Gustav Kirchhoff. Ueber den einfluss der wärmeleitung in einem gase auf die schallbewegung. *Annalen der Physik*, 210(6):177–193, 1868.

[6] MCAM Peters, Avraham Hirschberg, AJ Reijnen, and APJ Wijnands. Damping and reflection coefficient measurements for an open pipe at low mach and low helmholtz numbers. *Journal of Fluid Mechanics*, 256:499–534, 1993.

[7] E Dokumaci. On attenuation of plane sound waves in turbulent mean flow. *Journal of Sound and Vibration*, 320(4-5):1131–1136, 2009.

[8] Hugh Goyder. Damping of acoustic waves in pipelines due to end conditions. In *ASME 2013 Pressure Vessels and Piping Conference*, pages V004T04A036–V004T04A036. American Society of Mechanical Engineers, 2013.

[9] C. Lahiri, K. Knobloch, F. Bake, and L. Enghardt. Attenuation of sound in wide ducts with flow at elevated pressure and temperature. *Journal of Sound and Vibration*, 333(15):3440 – 3458, 2014.

[10] D Rockwell and Et Naudascher. Self-sustaining oscillations of flow past cavities. *Journal of Fluids Engineering*, 100(2):152–165, 1978.

[11] Mahmoud Shaaban and Atef Mohany. Passive control of flow-excited acoustic resonance in rectangular cavities using upstream mounted blocks. *Experiments in Fluids*, 56(4):72, 2015.

[12] Ahmed Omer, Nadim Arafa, Atef Mohany, and Marwan Hassan. The effect of upstream edge geometry on the acoustic resonance excitation in shallow rectangular cavities. *International Journal of Aeroacoustics*, 15(3):253–275, 2016.

[13] Hans R Graf and Samir Ziada. Excitation source of a side-branch shear layer. *Journal of Sound and Vibration*, 329(14):2825–2842, 2010.

[14] D Rockwell and E Naudascher. Self-sustained oscillations of impinging free shear layers. *Annual Review of Fluid Mechanics*, 11(1):67–94, 1979.

[15] Nadim Arafa and Atef Mohany. Aeroacoustic response of a single cylinder with straight circular fins in cross-flow. *Journal of Pressure Vessel Technology*, 137(5):051301, 2015.

[16] Nadim Arafa and Atef Mohany. Flow-excited acoustic resonance of isolated cylinders in cross-flow. *Journal of Pressure Vessel Technology*, 138(1):011302, 2016.

[17] Nadim Arafa, Ahmed Tariq, Atef Mohany, and Marwan Hassan. Effect of cylinder location inside a rectangular duct on the excitation mechanism of acoustic resonance. *Canadian Acoustics*, 42(1):33–40, 2014.

[18] Mohammed Alziadeh and Atef Mohany. Near-wake characteristics and acoustic resonance excitation of crimped spirally finned cylinders in cross-flow. *Journal of Pressure Vessel Technology*, 140(5):051301, 2018.

[19] M Alziadeh and A Mohany. Passive noise control technique for suppressing acoustic resonance excitation of spirally finned cylinders in cross-flow. *Experimental Thermal and Fluid Science*, 102:38–51, 2019.

[20] Samir Ziada. Control of fluid-structure-sound interaction mechanisms by means of synthetic jets. *JSME International Journal Series C Mechanical Systems, Machine Elements and Manufacturing*, 46(3):873–880, 2003.

[21] Ahmed Omer, Atef Mohany, and Marwan Hassan. Effect of impingement edge geometry on the acoustic resonance excitation and strouhal numbers in a ducted shallow cavity. *Wind and Structures*, 23(2):91–107, 2016.

[22] M Shaaban, M Abdelmwgoud, N Arafa, K Sachedina, A Mohany, and M Hassan. Measurements of acoustic admittance of piping systems at different flow velocities. In *37th annual Canadian Nuclear Society Conference*, 2017.

[23] Jian Jun Shu, Clifford R Burrows, and Kevin A Edge. Pressure pulsations in reciprocating pump piping systems part 1: modelling. *Proceedings of the Institution of Mechanical Engineers, Part I: Journal of Systems and Control Engineering*, 211(3):229–235, 1997.

[24] M Morgenroth and DS Weaver. Sound generation by a centrifugal pump at blade passing frequency. *Journal of turbomachinery*, 120(4):736–743, 1998.

[25] V Chatoorgoon and Qizhao Li. A study of acoustic wave damping in water-filled pipes with zero flow and turbulent flow. *Nuclear Engineering and Design*, 239(11):2326–2332, 2009.

[26] Bo Gao, Ning Zhang, Zhong Li, Dan Ni, and MinGuan Yang. Influence of the blade trailing edge profile on the performance and unsteady pressure pulsations in a low specific speed centrifugal pump. *Journal of Fluids Engineering*, 138(5):051106, 2016.

[27] Ga Rzentkowski and Sb Zbroja. Experimental characterization of centrifugal pumps as an acoustic source at the blade-passing frequency. *Journal of Fluids and Structures*, 14(4):529–558, 2000.

[28] Juan Manuel De Bedout, MA Franchek, RJ Bernhard, and L Mongeau. Adaptive-passive noise control with self-tuning helmholtz resonators. *Journal of Sound and Vibration*, 202(1):109–123, 1997.

[29] Edward J Brambley. Well-posed boundary condition for acoustic liners in straight ducts with flow. *AIAA journal*, 49(6):1272–1282, 2011.

[30] CD Field and FR Fricke. Theory and applications of quarter-wave resonators: A prelude to their use for attenuating noise entering buildings through ventilation openings. *Applied Acoustics*, 53(1-3):117–132, 1998.

[31] Omar Sadek, Mahmoud Shaaban, and Atef Mohany. Suppression of acoustic resonance in piping system using passive control devices. *Journal of Canadian Acoustic*, 42(3):58–59, 2014.

[32] A Selamet, NS Dickey, and JM Novak. The herschel–quincke tube: a theoretical, computational, and experimental investigation. *The Journal of the Acoustical Society of America*, 96(5):3177–3185, 1994.

[33] Mikael Karlsson, Ragnar Glav, and Mats Åbom. The herschel–quincke tube: The attenuation conditions and their sensitivity to mean flow. *The Journal of the Acoustical Society of America*, 124(2):723–732, 2008.

[34] GW Stewart. The theory of the herschel-quincke tube. *Physical Review*, 31(4):696, 1928.

[35] T Lato and A Mohany. Passive damping of pressure pulsations in pipelines using herschel-quincke tubes. *Journal of Sound and Vibration*, 448:160–177, 2019.

[36] PK Tang and WA Sirignano. Theory of a generalized helmholtz resonator. *Journal of Sound and Vibration*, 26(2):247–262, 1973.

[37] Dan Zhao and Aimee S Morgans. Tuned passive control of combustion instabilities using multiple helmholtz resonators. *Journal of sound and vibration*, 320(4-5):744–757, 2009.

[38] M Abdelmwgoud, M Shaaban, N Arafa, K Sachedina, A Mohany, and M Hassan. Use of helmholtz resonators to suppress acoustic pressure pulsations in pipelines. In *37th annual Canadian Nuclear Society Conference*, 2017.

[39] Ben T Zinn. A theoretical study of non-linear damping by helmholtz resonators. *Journal of Sound and Vibration*, 13(3):347–356, 1970.

[40] A Selamet, P Mi Radavich, NS Dickey, and JM Novak. Circular concentric helmholtz resonators. *The Journal of the Acoustical Society of America*, 101(1):41–51, 1997.

[41] Uno Ingard. On the theory and design of acoustic resonators. *The Journal of the acoustical society of America*, 25(6):1037–1061, 1953.

[42] M Alster. Improved calculation of resonant frequencies of helmholtz resonators. *Journal of Sound and Vibration*, 24(1):63–85, 1972.

[43] RC Chanaud. Effects of geometry on the resonance frequency of helmholtz resonators. *Journal of Sound and Vibration*, 178(3):337–348, 1994.

[44] Ronald L Panton and John M Miller. Resonant frequencies of cylindrical helmholtz resonators. *The Journal of the Acoustical Society of America*, 57(6):1533–1535, 1975.

[45] A Selamet, NS Dicky, and JM Novak. Theoretical, computational and experimental investigation of helmholtz resonators with fixed volume: lumped versus distributed analysis. *Journal of sound and vibration*, 2(187):358–367, 1995.

[46] Ruolong Ma, Paul E Slaboch, and Scott C Morris. Fluid mechanics of the flow-excited helmholtz resonator. *Journal of Fluid Mechanics*, 623:1–26, 2009.

[47] PA Nelson, NA Halliwell, and PE Doak. Fluid dynamics of a flow excited resonance, part i: experiment. *Journal of Sound and Vibration*, 78(1):15–38, 1981.

[48] PA Nelson, NA Halliwell, and PE Doak. Fluid dynamics of a flow excited resonance, part ii: Flow acoustic interaction. *Journal of sound and vibration*, 91(3):375–402, 1983.

[49] JS Anderson. The effect of an air flow on a single side branch helmholtz resonator in a circular duct. *Journal of sound and vibration*, 52(3):423–431, 1977.

[50] SK Tang. On sound transmission loss across a helmholtz resonator in a low mach number flow duct. *The Journal of the Acoustical Society of America*, 127(6):3519–3525, 2010.

[51] Xu Wang and Cheuk-Ming Mak. Wave propagation in a duct with a periodic helmholtz resonators array. *The Journal of the Acoustical Society of America*, 131(2):1172–1182, 2012.

[52] Xu Wang and Cheuk-Ming Mak. Disorder in a periodic helmholtz resonators array. *Applied acoustics*, 82:1–5, 2014.

[53] Chenzhi Cai, Cheuk Ming Mak, and Xu Wang. Noise attenuation performance improvement by adding helmholtz resonators on the periodic ducted helmholtz resonator system. *Applied Acoustics*, 122:8–15, 2017.

[54] Chenzhi Cai and Cheuk Ming Mak. Noise control zone for a periodic ducted helmholtz resonator system. *The Journal of the Acoustical Society of America*, 140(6):EL471–EL477, 2016.

[55] ML Munjal and AG Doige. Theory of a two source-location method for direct experimental evaluation of the four-pole parameters of an aeroacoustic element. *Journal of Sound and Vibration*, 141(2):323–333, 1990.

[56] Z Tao and AF Seybert. A review of current techniques for measuring muffler transmission loss. *SAE transactions*, pages 2096–2100, 2003.

[57] Finn Jacobsen. *Propagation of sound waves in ducts*. 2000.

[58] Manchar Lal Munjal. *Acoustics of ducts and mufflers with application to exhaust and ventilation system design*. John Wiley & Sons, 2014.

[59] Lewis H Bell. Industrial noise control. *Mechanical Engineering-New York And Basel*, 88:417–426, 1993.

[60] E ASTM. 1050. *Standard test method for impedance and absorption of acoustical materials using a tube, two microphones, and a digital frequency analysis system*, 1998.

[61] Harold Levine and Julian Schwinger. On the radiation of sound from an unflanged circular pipe. *Physical review*, 73(4):383, 1948.

[62] JY Chung and DA Blaser. Transfer function method of measuring in-duct acoustic properties. ii. experiment. *The Journal of the Acoustical Society of America*, 68(3):914–921, 1980.

[63] S.S. Rao. *Mechanical Vibrations*. World student series. Addison-Wesley, 1995.

[64] X Wang and CM Mak. Acoustic performance of a duct loaded with identical resonators. *The Journal of the Acoustical Society of America*, 131(4):EL316–EL322, 2012.

[65] Sabry Allam and Mats Åbom. Investigation of damping and radiation using full plane wave decomposition in ducts. *Journal of sound and vibration*, 292(3-5):519–534, 2006.

[66] U Ingård and S Labate. Acoustic circulation effects and the nonlinear impedance of orifices. *The Journal of the Acoustical Society of America*, 22(2):211–218, 1950.

[67] Uno Ingard and Hartmut Ising. Acoustic nonlinearity of an orifice. *The journal of the Acoustical Society of America*, 42(1):6–17, 1967.

[68] AS Hersh, BE Walker, and JW Celano. Helmholtz resonator impedance model, part 1: Nonlinear behavior. *AIAA journal*, 41(5):795–808, 2003.

[69] KS Andersen. Analyzing muffler performance using the transfer matrix method. In *COMSOL Conf., Hannover*, 2008.

[70] JY Chung and DA Blaser. Transfer function method of measuring in-duct acoustic properties. i. theory. *The Journal of the Acoustical Society of America*, 68(3):907–913, 1980.

[71] SJ Kline and FA McClintock. Describing uncertainties in single-sample experiments. *Mechanical Engineering*, 75(1):3–8.

Appendix A

Uncertainty Analysis

The calculated values presented in the results of this thesis are subject to uncertainty caused by potential errors in the measured values. This section highlights the expected sources of error and quantifies the uncertainty in calculated values where appropriate.

Uncertainty in the transmission loss arises from errors in microphone spacing measurements, estimation of the speed of sound, and the transfer function calculations. It should be noted, however, that mismatch errors within the calculated transfer functions can be corrected using the procedures outlined by Chung and Blaser [70], which account for both gain and phase mismatch between two measurement channels. Furthermore, Munjal and Doige [55] note that the unequal frequency response (bias error) between channels can be eliminated by calibration. Following these procedures, the only uncertainty arising from the microphone measurements is caused by random errors, which were minimized by running each experimental trial for 90 seconds and performing ensemble averaging of the results.

Since the two source location method was employed, uncertainties in the four poles (or elements) of the transfer matrix, from which the transmission loss is calculated, can be evaluated. For example, consider transfer matrix element $T_{11,23}$, which is obtained

using Equations 3.3 and 3.4 (see Chapter 3):

$$T_{11,23} = \frac{\Delta_{34}(H_{23a}H_{43b} - H_{23b}H_{43a}) + T_{22,34}(H_{23b} - H_{23a})}{\Delta_{34}(H_{43b} - H_{43a})} \tag{A.1}$$

where H_{ij} is the transfer function for microphone locations i and j, at speaker location a or b. The uncertainty in this pole due to an error in an independent variable x can be expressed [55]:

$$(\delta T_{11,23})_x = \frac{\partial T_{11,23}}{\partial x}\delta x \tag{A.2}$$

The uncertainty in each of the four transfer matrix elements arising from errors in the measured values can therefore be calculated using this method. As an example, element $T_{11,23}$ is considered for the zero mean flow velocity case. The uncertainty due to error in the speed of sound, c, can be calculated using:

$$(\delta T_{11,23})_c = \frac{2\pi f \cdot s(H_{23b} - H_{23a})sin(2\pi f/c \cdot s)}{c^2(H_{43b} - H_{43a})}\delta c \tag{A.3}$$

where the uncertainty in c is approximately 2 m/s, i.e. $\delta c = \pm 2$ m/s, which is caused by temperature fluctuations and errors in temperature measurement. Uncertainty caused by errors in the measured microphone spacing, s, is given by:

$$(\delta T_{11,23})_s = -\frac{2\pi f(H_{23b} - H_{23a})sin(2\pi f/c \cdot s)}{c(H_{43b} - H_{43a})}\delta s \tag{A.4}$$

where the error in the microphone spacing is 2.5 mm, i.e. $\delta s = \pm 2.5$ mm. The uncertainties caused by the measured transfer functions can be found using the following equations:

$$(\delta T_{11,23})_{H_{23a}} = \frac{-H_{43a} + cos(2\pi f/c \cdot s)}{H_{43b} - H_{43a}}\delta H_{23a} \tag{A.5}$$

$$(\delta T_{11,23})_{H_{23b}} = \frac{H_{43b} - cos(2\pi f/c \cdot s)}{H_{43b} - H_{43a}}\delta H_{23b} \tag{A.6}$$

$$(\delta T_{11,23})_{H_{43a}} = -\frac{(H_{23b} - H_{23a})(H_{43b} - cos(2\pi f/c \cdot s))}{(H_{43b} - H_{43a})^2}\delta H_{43a} \tag{A.7}$$

$$(\delta T_{11,23})_{H_{43b}} = \frac{(H_{23b} - H_{23a})(H_{43a} - cos(2\pi f/c \cdot s))}{(H_{43b} - H_{43a})^2}\delta H_{43b} \tag{A.8}$$

where the uncertainty associated with each of the transfer functions is ± 1 %.

In order to quantify the total error in a calculated result, R, which is a function of the independently measured values $x_1, x_2, ..., x_n$, the Kline and McClintock method [71] can be used, according to:

$$\delta R = \left\{ \sum_{i=1}^{n} \left(\frac{\partial R}{\partial x_i} \delta x_i \right)^2 \right\}^{1/2} \tag{A.9}$$

This method can be employed to determine the effects of uncertainty on the other transfer matrix elements. An estimation of the uncertainty in the four poles was obtained by calculating the uncertainty caused by each of the independent measured parameters discussed above for sample experimental data. An estimation of the resulting maximum uncertainties are summarized in Table A.1. The error at 150 Hz was calculated since it is the frequency of interest.

Table A.1: Approximate maximum uncertainties in calculated transfer matrix coefficients and transmission loss.

Calculated value	**Uncertainty**
$T_{11,23}$	1.44 %
$T_{12,23}$	0.013 %
$T_{21,23}$	3.10 %
$T_{22,23}$	1.92 %
Transmission Loss	1.79 %

Uncertainty in insertion loss measurements is simply a function of the sensitivity of the microphones and their calibration. Calibration was performed using a pistonphone calibrator, which generates a known excition level at a discrete frequency. For the sound

pressure amplitudes considered, the maximum error in a single sound pressure level measurement is approximately 0.5 dB, i.e. $\delta SPL = 0.5$ dB. Therefore, for the insertion loss, which is calculated from the difference between two SPL measurements, the maximum expected error is 1 dB.